NASA Contractor Report 189069

Self Adaptive Solution Strategies: Locally Bound Constrained Newton Raphson Solution Algorithms

Joe Padovan
University of Akron
Akron, Ohio

November 1991

Prepared for
Lewis Research Center
Under Grant NAG3–54

National Aeronautics and
Space Administration

TABLE OF CONTENTS

I. INTRODUCTION

In recent years, significant activities have been undertaken to improve the efficiency, stability and range of application of Newton Raphson (NR) type solution schemes in handling nonlinear finite element (FE) simulations. This has led to the development of hyperlinear [1,2], circular [3], elliptic [4,5] and piecewise continuous [6] constraint surfaces. These are used to control the INR iterative process, thereby, enabling the handling of transition in Jacobian definiteness, as well as, a wide variety of geometric and material nonlinearities [1-7]. Such work has emphasized the following developmental aspects namely:

i) Streamline Jacobian (stiffness matrix) updating for instance as in the use of the BFGS scheme [8-10];

ii) Introduce use of constraints to bound iterations associated with the incremental Newton Raphson (INR) algorithm, thus, enabling the handling of problem with indefinite Jacobian properties [3-6]; and

iii) Introduce self adaptive attributes enabling automatic load stepping [5,6].

The above work, in particular the constrained methodology has significantly extended the range of INR based schemes, regardless several difficulties are still present. In addition to the storage intensiveness of the scheme, the user is faced with the lack of apriori or automatic procedures enabling adjustment of size, shape and orientation of the constraint surface, so as to enhance numerical robustness. In this context, the user must undergo the trial and error process of defining

load stepping. Depending on the constraint function employed, this involves the specification of the various geometric attributes of the bounding surface. For instance, in the case of the hyperelliptic constraint surface (HECS), the aspect ratio and overall ordinate and abscissa bounds must be established on a global level.

To circumvent the foregoing difficulties, this paper develops numerical strategies which enable the automatic adjustment of the size, shape and orientation of the constraint surface associated with full (FINR), modified (MINR) and BFGS updated Newton Raphson FE equation solvers. This will be achieved through the introduction of a hierarchy of localized constraints which enable the control of the iterative excursions of various levels of the governing field variables. The approach taken is general in that a wide variety of constraint surfaces can be handled by the methodology. In addition to the general development, the results of several extensive benchmark activities is also presented. Here, special emphasis is given to illustrating the flexibility and robustness of the locally bound approach to controlling successive globally constrained INR type solution algorithms. In the sections which follow, detailed discussions will be given on the nature and extent of shortcomings of constrained approaches, the development of reshaping and resizing schemes from a 1-D point of view, the development of local constraint methodologies via FE generalization. Finally, the results of extensive benchmark examples demonstrating enhanced numerical characteristics will be presented.

II. CONSTRAINED NEWTON RAPHSON SCHEMES: STRENGTHS/SHORTCOMINGS

As noted earlier, INR type solution schemes involving either modified, straight or BFGS type stiffness updating suffer from several

very basic shortcomings [11]. To simplify the discussion and development, the INR is reinterpreted to be a linearly bound hyperlinear extrapolation of the solution curve via a full, modified or BFGS updated stiffness. Specifically, noting Fig. 2-1, the succession of extrapolation are bound by the intersection with the hyperplane defined by the designated load level. For such a process, it is difficult to guarantee the requisite intersections. This is especially true for structural stability problems involving buckling with turning point behavior where slope indefiniteness may occur.

To bypass such problems, the surface bounding the INR extrapolation can be reinterpreted to be a hyperplane which is oblique to $\underset{\sim}{F}$ = constant or alternatively a different function. Such an interpretation naturally yields the approaches taken by Wempner [1], Riks [2], Crisfield [3] and Padovan, et al. [4-6]. Specifically, noting Fig. 2-2, this has led to the use of constant arc lengths [1,2], oblique hyperlines, and circular [3], elliptic [4,5], hyperbolic [6], as well as, piecewise continuous [6] bounding constraint surfaces. While all such methodologies can handle the turning point problems associated with structural stability, as shown in Fig. 2-3, those which involve closed constraint curves more readily guarantee the requisite intersection with the INR extrapolation [5].

In spite of the advanced features of the foregoing schemes, the constrained approach also suffers from several very important fundamental shortcomings. While various of these are still outgrowths of the methodologies INR base, several are a direct function of the use of the constraint concept. Overall, the shortcomings are defined by the following:

i) Unlike the $\underset{\sim}{F}$ = constant constraint surface, all the other surfaces yield intersections with the INR extrapolations which,

due to system nonlinearity remain apriori unknown; this makes the calculation for specific so called target loads awkward.

ii) While the various constraint surfaces self adaptively adjust load stepping during successive iterations, such incrementation is a direct outgrowth of their intrinsic geometries. Hence, the user is still left with the oftentimes puzzling problem of defining their requisite shape, aspect ratio, obliqueness, arc length, radii, etc.

iii) Because of the lack of apriori knowledge of the intersection of the constraint and INR extrapolation, it is difficult to handle mixed problems which may involve some combination of prescribed displacement and loading requirements or targets.

iv) Oversized constraint surfaces may initiate a nonintersection in hyperspace and hence solution failure. (See Fig. 2-4). In contrast, an overly tight surface can result in an inefficient and hence, expensive iteration process.

v) Generally, since the intersections of the constraint curve and solution surface are not apriori known, typically the constrained methodology will converge to points significantly reduced from expected load steps: Noting Fig. 2-5, this leads to under utilized load steps and consequently numerical inefficiency.

In the following sections, several methodologies will be implemented to bypass the foregoing shortcomings. As will be seen, these are general enough to be employed with most of the constraints in use today.

III. IMPROVED CONSTRAINT SCHEME: 1-D DEVELOPMENT

To simplify the development of the improved constraint methodology, we shall first consider modifications to the solution of 1-D nonlinear equations. Recalling the comments of the preceding section, it follows that the shortcomings of the NR based constraint schemes fall into several main categories namely:

i) The need to develop methodologies which -
   - Enable convergence to specific load and/or deflection states and;
   - Allow full use of a given load step;

ii) Develop schemes which automate -
   - Sizing of constraint surface and;
   - Reshape and reorient constraint surface so as to improve convergence characteristics.

To circumvent the foregoing shortcomings, several different modifications will be introduced into the constrained methodology. The main thrust of these will be twofold, namely:

i) To provide for self adaptive modifications of constraint geometry enabling convergence to designated target load and/or deflection state and;

ii) To employ localized constraints so as to enable essentially automatic sizing of constraint while still maintaining numerically stable convergence characteristics.

While the geometries of the various candidate constraint hyper-surfaces are unique, there are basic coordinate transformations which will enable flexible reshaping and reorientation. Specifically, for

this paper, we shall consider the use of translations, rotations and coordinate stretches. Obviously, dependent on the type of constraint geometry used, some of these schemes are more advantageous than others. For example, consider the use of the oblique hyperplane, Fig. 3-1 illustrates combinations of rotation and rotation-translations. While both schemes possess the requisite targeting capabilities, the piecewise continuous rotation-translation scheme may yield a more stable numerical convergence process. Note, in the vicinity of turning points, the rotation process of both methodologies would have to be stopped to guarantee an intersection with the solution curve.

Considering the piecewise hyperbolic constraint, Fig. 3-2 demonstrates the use of translations to enable requisite targeting. As with the oblique hyperplanar constraint, in the vicinity of turning points, the translation process is stopped to insure the requisite intersections.

For the elliptic constraint, abscissa or ordinate coordinate stretches can be used to enable the requisite targeting. Such a process is illustrated in Fig. 3-3. In particular, the iterations depicted involve an abscissa stretched hyperelliptic constraint surface AHECS.

To establish the requisite algorithmic formulation, we shall consider the following 1-D nonlinear equation namely:

$$G(Y) = F \tag{3.1}$$

The NR scheme associated with (3.1) is given by the expression

$$Y_{n+1} = Y_n + (\phi - G(Y_n))/G'(Y_n)\ ;\ G'(Y_n) = \frac{d}{dY}\,(G(Y_n)) \tag{3.2}$$

such that ϕ is the designated value of F. In terms of the constraint

concept, the iterations defined by (3.2) can be bound by rescaling ϕ via the parameter λ. The choice of λ is given by the intersection of the NR extrapolation and the constraint curve. For example, such intersections are defined in Fig. 2-2. Overall, such a process is given by the following relations:

i) Constrained NR algorithm;

$$Y_{n+1} = Y_n + (\lambda_{n+1}\,\phi - G(Y_n))/G'(Y_n) \tag{3.3}$$

ii) Constraint curve;

$$C(Y, \phi) = 0 \tag{3.4}$$

Such that the intersection takes the form

$$I\,(\lambda_{n+1}, Y_{n+1}) = 0.$$

To determine λ_{n+1}, the specific form of C must be chosen. In the case of oblique linear, circular, elliptic and piecewise hyperbolic curves/surfaces, we have that [1-6]

i) Oblique linear

$$F = \alpha\, Y + \phi \tag{3.5}$$

ii) Circular

$$F^2 + Y^2 = \phi^2 \tag{3.6}$$

iii) Elliptic

$$F^2 + \mu Y^2 = \phi^2 \tag{3.7}$$

iv) Piecewise Hyperbolic

$$(F - \phi)(Y - \gamma) = \mu \tag{3.8}$$

where the parameters α, ϕ, γ and μ are user defined. As noted earlier, such relationships can be modified to admit translation rotation and coordinate stretching.

For instance, considering the oblique linear constraint, rotation can be introduced by varying the selection of α in the range $\alpha \in [0, \mu)$; $\mu < \infty$ for $\bar{F} > \bar{0}$ and $\alpha \in [-\mu, 0)$; $\mu < \infty$ for $\bar{F} \leq \bar{0}$. The actual variation of α can be undertaken in several different ways, namely

i) Angular increments, Fig. 3-4;

ii) Force increments, Fig. 3-5;

iii) MNR estimated $\Delta\bar{Y}$, Fig. 3-6;

iv) BFGS-NR estimated $\Delta\bar{Y}$, and via

v) BFGS-NR or MNR estimated ΔF.

Note in the case of fixed $\Delta\bar{Y}$ incrementation, the sweeping of the oblique linear constraint is modified to handle iterative steps in the vicinity of the designated load and/or deflection state. Specifically, the constraint is set to $F = \phi$. Overall, the algorithm associated with the fixed MNR estimated $\Delta\bar{Y}$ sweep of the oblique linear constraint requires a knowledge of successive intersection points. That is, considering the $(n+1)^{th}$ rotation, the associated MNR extrapolation and oblique linear constraint curve are given by the following relations:

$$Y = Y_n + (F - G(Y_n))/G' \tag{3.9}$$

and

$$F = \alpha_{n+1} Y + \phi \tag{3.10}$$

In terms of (3.9) and (3.10), the intersection I_n' defined in Fig. 3-7 is given by

$$Y_n' = Y_n^\circ + (\lambda_{n+1}' \Phi - G(Y_n^\circ))/G' \tag{3.11}$$

$$\lambda_{n+1}' \Phi = \alpha_{n+1} Y_n' + \Phi \tag{3.12}$$

Since

$$Y_n' - Y_n^\circ = \Delta\bar{Y} \tag{3.13}$$

is given, (3.11) and (3.12) can be used to define the unknowns α_{n+1} and λ_{n+1}'. After several manipulations we have that

$$\alpha_{n+1} = \frac{1}{Y_n^\circ + \Delta\bar{Y}} \{G' \Delta\bar{Y} + G(Y_n^\circ) - \Phi\} \tag{3.14}$$

$$\lambda_{n+1}' = \frac{1}{\Phi(Y_n^\circ + \Delta\bar{Y})} \{G' \Delta\bar{Y} + G(Y_n^\circ) - \Phi\} \tag{3.15}$$

Note, for the BFGS or fully updated schemes, G' appearing in (3.14) and (3.15) can be replaced by its corrected values namely $G'(Y_n)$.

The swept oblique linearly constrained MNR algorithm has two basic forms. Namely for $\lambda_{n+1}' < 1$, (3.14) and (3.15) are used to perform the necessary iterations. When $\lambda_{n+1}' > 1$, then sweeping is stopped and iteration continues as per (3.2). Note, in the vicinity of turning or buckling points, the foregoing algorithm must be modified to insure the requisite intersection. This can be achieved in several ways that is:

i) The curvature can be monitored as per the $G'(Y_n)$ parameter; when below critical level sweeping is stopped;

ii) Alternatively, a monotonicity check of the $G(Y_n)$ sequence can be used to terminate sweeping.

In a similar context, the alternative constraint curves can be modified to include rotations, translations and stretches. For example, we shall consider the more versatile elliptic surface defined in Figs. 2-5 and 3-3. Considering the $(n+1)^{th}$ successive stretch depicted in Fig. 3-8, the following relations define the intersection I_n' namely

$$Y_n' = Y_n^\circ + (\lambda_{n+1}' \phi - G(Y_n^\circ))/G' \tag{3.16}$$

$$(\lambda_{n+1}' \phi)^2 + \mu_{n+1} (Y_n')^2 = \phi^2 \tag{3.17}$$

Due to (3.13), solving (3.16) and (3.17) for λ_{n+1}' and μ_{n+1} we have that

$$\lambda_{n+1}' = \frac{1}{\phi} \{G' \Delta\bar{Y} + G(Y_n^\circ) \} \tag{3.18}$$

$$\mu_{n+1} = \frac{1}{(Y_n^\circ + \Delta\bar{Y})^2} \{\phi^2 - (G' \Delta\bar{Y} - G(Y_n^\circ))^2 \} \tag{3.19}$$

Like the oblique linear constraint, the elliptically bound NR can be employed in a variety of ways. These include:

i) After each stretch of the elliptic constraint curve, several iterations can be used to stabilize the numerical convergence process;

ii) The ongoing stretch of the elliptic constraint can be used to delimit successive INR type iterations;

iii) The constraint can be employed with either BFGS, full or modified slope updating;

iv) For $\lambda_n^{\ell} \sim O(1)$, $\Delta\bar{Y}$ can be set to ∞ (large number) to enable convergence to designated load level;

v) When the definiteness of G' varies as in the vicinity of turning points, the stretching process is terminated.

As noted by Padovan and Arechaga [5] so-called safety zones can be established for the constrained scheme wherein convergence can be guaranteed under the appropriate conditions. For instance, let us consider the case where successive iterations are undertaken between abscissa or ordinate stretches of the ellipse. Recalling (3.16) and (3.17), once μ_{n+1} is fixed by the stretch, (3.19), we must insure that subsequent iterations lie in the appropriate safety zone. This is determined by monitoring the intersection points of subsequent iterations. Specifically, noting Fig. 3-8, it follows that the ℓ^{th} intersection of the n^{th} ordinate stretch is given by

$$Y_n^{\ell} = Y_n^{\ell-1} + (\lambda_{n+1}^{\ell}\,\phi - G(Y_n^{\ell-1}))/G' \tag{3.20}$$

$$(\lambda_{n+1}^{\ell}\,\phi)^2 + \mu_{n+1}\,(Y_n^{\ell})^2 = \phi^2 \tag{3.21}$$

Solving for λ_{n+1}^{ℓ} we obtain the following quadratic identity, that is

$$(\lambda_{n+1}^{\ell})^2\, C_{1\ell n} + 2\,\lambda_{n+1}^{\ell}\, C_{2\ell n} + C_{3\ell n} = 0 \tag{3.22}$$

where

$$C_{1\ell n} = \phi^2 + (\phi/G')^2\,\mu_{n+1} \tag{3.23}$$

$$C_{2\ell n} = (Y_n^{\ell-1} - G(Y_n^{\ell-1})/G')(\phi/G')\,\mu_{n+1} \tag{3.24}$$

$$C_{3\ell n} = (Y_n^{\ell-1} - G(Y_n^{\ell-1})/G')^2 \mu_{n+1} - \phi^2 \qquad (3.25)$$

In terms of (3.22), we yield the expression

$$\lambda_{n+1}^{\ell} = \frac{1}{C_{1\ell n}} \{ - C_{2\ell n} \pm [(C_{2\ell n})^2 - C_{1\ell n} C_{3\ell n}]^{\frac{1}{2}} \} \qquad (3.26)$$

Following the formalism of Padovan and Arechaga [5], for the current purposes, the safety zone is defined by those values of Y and F where the discriminant of (3.26) is positive definite. Noting (3.23) - (3.24), such a requirement yields that

$$(C_{2\ell n})^2 \geq C_{1\ell n} C_{3\ell n} \rightarrow$$

$$(Y_n^{\ell+1} - G(Y_n^{\ell-1})/G')^2 (\phi/G')^2 (\mu_{n+1})^2 \geq$$

$$(\phi^2 + (\phi/G')^2 \mu_{n+1}) \{ (Y_n^{\ell-1} - G(Y_n^{\ell-1})/G')^2 \mu_{n+1} - \phi^2 \} \qquad (3.27)$$

Such a criterion enables the appropriate choice of $\Delta\bar{Y}$ and hence the sizing of the ellipse.

The foregoing discussion has developed a variety of methodologies enabling the convergence to specified force and/or deflection states. Generally, this has involved the reshaping or sizing of the constraint surface. In the section to follow, the scheme will be automated through the use of localized constraints which retain targeting capabilities, while also enabling generalization to large scale multidegree of freedom simulations.

IV. EXTENSIONS TO N-D: FE DEVELOPMENT

To automate the control of the resizing/reshaping of the constraint surface for multidimensional problems, the use of localized bounds will be introduced. This will be facilitated by employing a nonlinear FE formulation. Specifically, assuming that the standard 2nd Piola Kirchhoff [13] stress S_{ij} and Lagrangian strain [13] L_{ij} tensor combination are employed, the governing field equations take the form

$$\frac{\partial}{\partial a_j} \left(S_{jk}\left(\delta_{ik} + \frac{\partial u}{\partial a_k}\right)\right) + f_{oi} = 0 \tag{4.1}$$

$$S_{ij} = S_{ij}\,(L_{11}, L_{22}, \ldots) \tag{4.2}$$

such that [13]

$$S_{ij} = \frac{\rho_o}{\rho} \frac{\partial a_i}{\partial x_\alpha} \frac{\partial a_j}{\partial x_\beta} \sigma_{\beta\alpha} \tag{4.3}$$

$$L_{ij} = \frac{1}{2}\,(u_{i,j} + u_{j,i} + u_{\ell,i}\ u_{\ell,j}) \tag{4.4}$$

with ρ_o, ρ defining the initial and current densities, x_i Euler coordinates, a_i Lagrangian coordinates, σ_{ij} the Cauchy stress and u_i are the components of the displacement vector. For nonlinear materials, generally (4.2) is cast in an incremental form. In this context

$$\Delta S_{ij} = \gamma_{ij\ell k}\ \Delta L_{\ell k} \tag{4.5}$$

such that $\gamma_{ij\ell k}$ is the tangent stiffness of the medium.

Using the usual displacement type formulation, the displacement vector of a given element can be related to its associated nodal de-

formations via the expression [14]

$$\underset{\sim}{u} = [N(\underset{\sim}{x})]\ \underset{\sim}{Y} \tag{4.6}$$

such that

$$\underset{\sim}{u}^T = (u_1, u_2, u_3) \tag{4.7}$$

and $[N]$, $\underset{\sim}{Y}$ respectively denote the shape function and nodal deflection column vector. Employing (4.1 - 4.7) inconjunction with the virtual work principle, the following FE formulations are obtained namely [14]

$$\int_R \delta(L)\ \underset{\sim}{S}\ dv \rightarrow$$

$$\int [B^*]^T\ \underset{\sim}{S}\ dv = \underset{\sim}{F} \tag{4.8}$$

where $\underset{\sim}{F}$ is a column vector defining nodal forces, $\delta(\ )$ the variational operator and

$$(\underset{\sim}{S})^T = (S_{11}, S_{22}, S_{33}, S_{12}, S_{23}, S_{13}) \tag{4.9}$$

$$\delta(\underset{\sim}{L}) = [B^*]\ \delta(\underset{\sim}{Y}) \tag{4.10}$$

with [4]

$$[B^*] = [B] + [B_n\ (\underset{\sim}{Y})]\ [G] \tag{4.11}$$

$$(\underset{\sim}{L})^T = (L_{11}, L_{22}, L_{33}, L_{12}, L_{23}, L_{13}) \tag{4.12}$$

The straight INR algorithm typically used to solve (4.8) is given by the expression [14,15]

$$[K\ (\underset{\sim}{Y}^k_m)]\ \Delta\underset{\sim}{Y}^k_{m+1} = \underset{\sim}{\Psi}^k_{m+1} \tag{4.13}$$

where k defines the load step, m the iteration count for the given step and [14,15]

$$\underset{\sim}{\Psi}^{k}_{m+1} = \underset{\sim}{F}^{k} - \int_{R} [B^{*}(\underset{\sim}{Y}^{k}_{m})]^{T} \underset{\sim}{S}(\underset{\sim}{Y}^{k}_{m})\, dv \tag{4.14}$$

$$\underset{\sim}{F}^{k} = \underset{\sim}{F}^{k-1} + \Delta \underset{\sim}{F}^{k} \tag{4.15}$$

$$[K(\underset{\sim}{Y}^{k}_{m})] = \int_{R} \{[G]^{T} [S(\underset{\sim}{Y}^{k}_{m})][G] + [B^{*}(\underset{\sim}{Y}^{k}_{m})]^{T}[D(\underset{\sim}{Y}^{k}_{m})][B^{*}(\underset{\sim}{Y}^{k}_{m})] \}dv \tag{4.16}$$

such that $[S(\underset{\sim}{Y}^{k}_{m})]$ is the prestress matrix defined at $\underset{\sim}{Y}^{k}_{m}$ and $[D(\underset{\sim}{Y}^{k}_{m})]$ is the tangent material stiffness matrix namely

$$\Delta \underset{\sim}{S}^{k}_{m} = [D(\underset{\sim}{Y}^{k}_{m})][B^{*}(\underset{\sim}{Y}^{k}_{m})]\ \Delta \underset{\sim}{Y}^{k}_{m} \tag{4.17}$$

For the MINR, the tangent stiffness $[K(\underset{\sim}{Y})]$ is updated intermittently.

For the constrained INR, the $\Delta \underset{\sim}{Y}^{k}_{m+1}$ excursion is bound by global level surfaces cast in terms of normed field variables. Specifically, considering the HECS, we have from Fig. 4-1 that

$$\| \underset{\sim}{f} \|^{2} + \mu \| \underset{\sim}{y} \|^{2} = \| \Delta \underset{\sim}{F}^{k} \|^{2} \tag{4.18}$$

where the Euclidean norm takes the form

$$\| \underset{\sim}{y} \|^{2} = \sum_{i} (y_{i})^{2} \tag{4.19}$$

Typically, the choice of μ and the target load is user defined. As can be seen from (4.18), such variables represent global level parameters and hence, are difficult to select. In as much as normed constraint equations like (4.18) or its linear; circular, or piecewise hyperbolic counterparts represent mathematically convenient expressions, they do not provide for control at local levels. This follows from the fact that norms represent gross upper bounds on the various excursions. In this

context they provide neither information on nor control of individual degrees of freedom. This situation applies to all the various types of field variables namely the deflections, deformation gradients, stresses, strains, strain energy density, temperature, thermal gradients velocities, accelerations etc.

The foregoing difficulties can be partially circumvented by partitioning the governing dependent finite element vectorial field variables into a hierarchy of different groups. At the lowest position of the hierarchy are individual field variables. These can be located either at given nodes or integration points. The overall levels which such groups can be partitioned consists of:

i) Individual degrees of freedom;

ii) Vectorial and tensorial quantities at nodes and integration points;

iii) Whole elements and substructural regions;

iv) Locally averaged quantities as in nodal or integration point extrapolation-interpolations; and

v) Material and nonlinear groupings.

Based on such a partitioning concept, the global norm of say $\underset{\sim}{Y}$ is itself a summation of the various hierarchy of localized norms. In particular, $\| \underset{\sim}{Y} \|$ can be rearranged as follows:

$$(\| \underset{\sim}{Y} \|)^2 = \sum_{i} (Y_i)^2$$

$$= \sum_{\ell}^{M} (\| \underset{\sim}{Y}_{\ell} \|)^2 \qquad (4.20)$$

where the hierarchy of vectors $\underset{\sim}{Y}_{\ell}; \ell = 1, 2, \ldots$ define the various groups within the global vector $\underset{\sim}{Y}$ namely

$$\underset{\sim}{Y}^T = \{\underset{\sim}{Y}_1^T, \underset{\sim}{Y}_2^T, \underset{\sim}{Y}_3^T, \ldots\}$$

Similar hierarchies of groups can be established for all the dependent field variables.

Overall, (4.20) can be applied at two levels namely, globally and locally. At the global level, $\| \underset{\sim}{Y} \|$ can be both employed within a constraint used to say control the overall iteration process of the INR so as to enable handling of Jacobian indefiniteness, as well as, within convergence tests. On the local scale, the various groups $\underset{\sim}{Y}_\ell$ and their associated norms $\| \underset{\sim}{Y}_\ell \|$ can be employed to delimit excursions generated during the overall iteration process. Such a dual level approach enables a higher degree of solution control. As will be seen later, this enables the use of much larger load/deflection increments while still maintaining good convergence characteristics.

The foregoing partitioned norms can be used to establish localized constraints which scale the load stepping. Like the global level application, the local constraint can be chosen from a variety of function types namely constant, linear, circular, elliptic, piecewise hyperbolic or perhaps more general bounding functions. The manner of application depends somewhat on the field variable excursion being controlled. Regardless, several types of applications can be outlined. Overall, these can be categorized into two main types namely

i) Greatest local upper bounds; and

ii) Intermediate local bounds.

For both procedures, excursions in the various field variables are first obtained via the standard INR scheme with either full modified or BFGS [8] type updating. Note, in the case of greatest upper bound schemes, the

constraint is chosen so that successive iterations converge essentially to the bound set. For the intermediate scheme, the constraint is chosen so that convergence is directed to limit points in the interval set by the bound.

To illustrate such approaches we shall first consider the use of displacement type controls. In terms of successive iterate excursions, a local upper bound test (LUBT) is required to gage the various partitioned groups. Employing the usual Euclidian norm to the partitioned groups yields the following LUBT, that is

$$\| \Delta \underset{\sim}{Y}_{\ell} \| \leq \Delta_{\ell}; \ \ell \varepsilon [1, u] \tag{4.21}$$

such that Δ_{ℓ} defines the ℓ^{th} group upper bound. Its choice will be discussed later. If (4.21) is satisfied, then no rescaling of the load increment is necessary. In cases where (4.21) is violated, then a one parameter stretch/contraction is applied to the load step. In particular, (4.14) is recast in the form

$$\Psi_{m+1}^{k} = \lambda_{m+1}^{k} \{ \underset{\sim}{F}^{k-1} + \Delta \underset{\sim}{F}^{k} - \int_{R} [B^{*}(\underset{\sim}{Y}_{m}^{k})]^{T} S(\underset{\sim}{Y}_{m}^{k}) dv \} \tag{4.22}$$

where

$$\lambda_{m+1}^{k} = \begin{cases} \min \left(\dfrac{\Delta_{\ell}}{\| \Delta \underset{\sim}{Y}_{m\ell}^{k} \|} \right); \ \| \Delta Y_{m\ell}^{k} \| > \Delta_{\ell} \\ \\ 1; \ \| \Delta \underset{\sim}{Y}_{m\ell}^{k} \| \leq \Delta_{\ell} \end{cases} \tag{4.23}$$

$$\ell \varepsilon [1, u]$$

Note the upper bound constraint defined by (4.22 and 4.23) can either be continuously or intermittently updated. If intermittent updating occurs, then the λ^{k} family is fixed at the beginning of each load increment.

For intermediate type bounds, condition (4.21) can be employed to resize the global constraint surface. Such a process generally leads to a succession of iterate excursions which are "smaller" or more conservative than those obtained by the previous upper bound approach. As an example, consider the scaling of the abscissa dimension of say the HECS. This is achieved by adjusting the parameter μ which controls the aspect ratio. Specifically, based on (4.12), the initial iterative excursion associated with say the k^{th} increment takes the form

$$\underset{\sim}{\Delta Y}_1^k = [K(\underset{\sim}{Y}_o^k)]\ \underset{\sim}{\Psi}_1^k \tag{4.24}$$

Now requiring that (4.21) be satisfied for all partitions associated with $\underset{\sim}{Y}$, we obtain the following one parameter scaling of the HECS abscissa namely

$$\mu_1^k = \theta_1^k \frac{\| \underset{\sim}{\Delta F}^k \|^2}{\| \underset{\sim}{\Delta Y}_1^k \|^2} \tag{4.25}$$

where

$$\theta_1^k = \begin{cases} \min \left(\dfrac{\Delta_\ell}{\| \underset{\sim}{Y}_{1\ell}^k \|} \right); & \| Y_{1\ell}^k \| > \Delta_\ell \\ \\ 1; & \| \Delta\, Y_{1\ell}^k \| > \Delta_\ell \end{cases} \tag{4.26}$$

$$\ell \in [1, \mu]$$

Note for the modified abscissa rescaled HECS namely the AHECS, the constrained surface is updated at the beginning of each load step and is thereafter fixed during successive iteration steps associated with the given load increment.

To enable the appropriate load targeting, μ must be updated

during the iterative process. In this case (4.25 and 4.26) take the form

$$\mu_{m+1}^{k} = \frac{\| \Delta \underset{\sim}{F}^{k} \|^{2}}{\| \sum_{r}^{m+1} \Delta \underset{\sim}{Y}_{r}^{k} / \theta_{r}^{k} \|^{2}} \tag{4.27}$$

such that

$$\theta_{m+1}^{k} = \begin{cases} \min \left(\dfrac{\Delta_{\ell}}{\| \Delta \underset{\sim}{Y}_{m+1\ell}^{k} \|} \right); & \| \Delta \underset{\sim}{Y}_{m+1\ell}^{k} \| > \Delta_{\ell} \\ 1; & \| \Delta \underset{\sim}{Y}_{m+1\ell}^{k} \| \leq \Delta_{\ell} \end{cases} \tag{4.28}$$

Based on the foregoing scaling of μ, the abscissa dimension of the AHECS is independent of the load step. In this context, under local constraint control, successive iterative excursions of the deflection field are largely independent of load step size so long as very large $\Delta \underset{\sim}{F}^{k}$ increments are employed. Specifically, noting Fig. 4.2, as load increment size is increased, the hyper tangent plane associated with the AHECS is essentially vertical. In this context, the intersections of the INR extrapolation and the AHECS occur near the upper bound constraint on the displacement excursion. As will be seen from the forthcoming benchmark examples, the foregoing configurational properties of the AHECS enable a high degree of displacement targeting control, as well as, make the scheme largely load step size insensitive.

In the context of such properties, the AHECS with localized displacement constraint enables the solution to progress to the requisite loading target under controlled upper bounded iterative increments. Such a load stepping process is more natural since the anticipated deflection in the structure can easily be evaluated directly from design level blue-

print considerations which define clearances, fits, acceptable structural deformations etc.

Pursuing this line of thought further, since strain is functionally dependent on the various displacement gradients $\frac{\partial u_i}{\partial a_j}$, it also seems natural to employ localized constraints on admissible slope excursions. In terms of the FE formulation, it follows that the various $\frac{\partial u_i}{\partial a_j}$ can be recast in matrix format, that is

$$\frac{\partial}{\partial x_j}(\underset{\sim}{u}) = \frac{\partial}{\partial x_j}(\underset{\sim}{f}) = \frac{\partial}{\partial x_j}([N]\underset{\sim}{Y}); \; j = 1, 2, 3 \tag{4.29}$$

Based on (4.29), placing constraints on admissible $\frac{\partial u_i}{\partial x_j}$ leads to the following pointwise bound on $\underset{\sim}{Y}$, that is

$$\underset{\sim}{Y} = \frac{\partial}{\partial x_j}([N])^{-1} \frac{\partial}{\partial x_j}(\underset{\sim}{f}) \rightarrow$$

$$\| \underset{\sim}{Y} \| = \| \frac{\partial}{\partial x_j} ([N])^{-1} \frac{\partial}{\partial x_j} (\underset{\sim}{f}) \|$$

$$\leq \| \frac{\partial}{\partial x_j} ([N])^{-1} \| \; \| \frac{\partial}{\partial x_j} (\underset{\sim}{f}) \|$$

$$\leq \| \frac{\partial}{\partial x_j} ([N])^{-1} \| \; \Gamma_j \tag{4.30}$$

where Γ_j defines the upper bound on $\| \frac{\partial f}{\partial x_j} \|$. From an incremental point of view, we have that

$$\| \Delta \underset{\sim}{Y} \| \leq \| \frac{\partial}{\partial x_j} ([N])^{-1} \| \; \Delta \Gamma_j \tag{4.31}$$

for $\forall \; x \in R$. If (4.31) is averaged say over a given element, then we obtain the more usable expression

$$\| (\Delta Y^k_{m+1})^e \| \leq V_e \| \int (\frac{\partial}{\partial x_j} [N])^{-1} \, dv \| \Delta r_j \tag{4.32}$$

$$j = 1, 2, 3$$

where V_e is the volume of the e^{th} element and $(\Delta Y^k_{m+1})^e$ the associated incremental nodal deflection. As can be seen, (4.32) represents a element level partitioning of the bounding process.

In the context of (4.32), similar bounds can be defined for strains, stresses as well as strain energy excursions. For instance, recalling the definition of strain, in terms of (4.4, 4.6, 4.11) we see that

$$\Delta L^k_{m+1} = ([B] + [B_n(Y^k_{m+1})][G]) \, \Delta Y^k_{m+1} \tag{4.33}$$

Considering say the e^{th} element, the norm of (4.33) leads to the following bounds for admissible ΔY^k_{m+1} namely

$$\Delta Y^k_{m+1} = ([B] + [B_n(Y^k_{m+1})][G])^{-1} \, \Delta L^k_{m+1} \tag{4.34}$$

$$\| \Delta Y^k_{m+1} \| = \| ([B] + [B_n(Y^k_{m+1})][G])^{-1} \, \Delta L^k_{m+1} \|$$

$$\leq \| ([B] + [B_n(Y^k_{m+1})][G])^{-1} \| \; \| \Delta L^k_{m+1} \|$$

$$< \| ([B] + [B_n(Y^k_{m+1})][G])^{-1} \| \, \Xi \tag{4.35}$$

where Ξ defines the upper bound on $\| \Delta L^k_{m+1} \|$. Averaging over say the e^{th} element yields the more useable constraint

$$\| (\Delta Y^k_{m+1})^e \| \leq V_e \| \int_{V_e} [B^*] \, dv \| \Xi_e \tag{4.36}$$

Noting the relation for stress increments, the following normed bounds for

the admissible $(\Delta \underset{\sim}{Y}^k_{m+1})^e$ can be developed via (4.17) namely

$$(\Delta \underset{\sim}{}^k_{m+1})^e = ([D][B^*(\underset{\sim}{Y}^k_m)])^{-1}(\Delta \underset{\sim}{S}^k_{m+1})^e$$

$$\leq \| ([D][B^*(\underset{\sim}{Y}^k_m)])^{-1}(\Delta \underset{\sim}{S}^k_{m+1}) \|$$

$$\leq \| ([D][B^*(\underset{\sim}{Y}^k_m)])^{-1} \| \, \| (\Delta \underset{\sim}{S}^k_{m+1})^e \|$$

$$\leq \| ([D][B^*(\underset{\sim}{Y}^k_m)])^{-1} \| \, \varsigma \qquad (4.37)$$

such that ς defines the upper bound on $\| (\Delta \underset{\sim}{S}^k_{m+1})^e \|$. Equation (4.37) defines a pointwise bound on $\| (\Delta \underset{\sim}{Y}^k_{m+1})^e \|$. For general use, volume averaged values are perhaps more useful. In this context, averaging (4.37) over say the e^{th} element yields the bounding expression

$$\| (\Delta \underset{\sim}{}^k_{m+1})^e \| \leq V_e \| \left(\int [D][B^*(\underset{\sim}{Y}^k_m)] \, dv \right)^{-1} \| \, \varsigma \qquad (4.38)$$

Lastly, we shall develop constraints based on controlling successive increments of energy. For the present purposes, this will be considered on an element level. In particular, based on (4.8) and Fig. 4.3, the energy increment associated with the e^{th} element for the $(n+1)^{th}$ iteration is given by the following approximating trapezoid, that is

$$E^{ek}_{m+1} = \frac{1}{2} \{ (\underset{\sim}{F}^k_m)^e + (\underset{\sim}{F}^k_{m+1})^e \}^T (\Delta \underset{\sim}{Y}^k_{m+1})^e \qquad (4.39)$$

such that

$$(\underset{\sim}{F}^k_{m+1})^e \sim (\underset{\sim}{F}^k_m)^e + [k^e](\Delta \underset{\sim}{Y}^k_{m+1})^e \qquad (4.40)$$

In a normed sense, (4.39) can be recast in the following quadratic polynomial form in $\| \Delta \underset{\sim}{Y}^k_{m+1} \|$ namely

$$E^{ek}_{m+1} = ((\underset{\sim}{F}^k_m)^e + \frac{1}{2}[K^e](\Delta \underset{\sim}{Y}^k_{m+1})^e)^T(\Delta \underset{\sim}{Y}^k_{m+1})^e$$

$$E^{ek}_{m+1} \leq \| (\underset{\sim}{F}^k_m)^e \| \| (\Delta \underset{\sim}{Y}^k_{m+1})^e \| + \frac{1}{2} \| [k^e] \| \| (\Delta \underset{\sim}{Y}^k_{m+1})^e \| +$$

$$\| (\Delta \underset{\sim}{Y}^k_{m+1})^e \|^2 + 2 \frac{\| (\underset{\sim}{F}^k_m)^e \|}{\| [K^e] \|} \| (\Delta \underset{\sim}{Y}^k_{m+1})^e \| - \frac{2E^{ek}_{m+1}}{\| [k^e] \|} > 0 \qquad (4.41)$$

Solving for $\| (\Delta \underset{\sim}{Y}^k_{m+1})^e \|$, we obtain the following element level constraint

$$\| (\Delta \underset{\sim}{Y}^k_{m+1})^e \| \leq \frac{\| (\underset{\sim}{F}^k_m)^e \|}{\| [k^e] \|} \pm$$

$$\sqrt{\left(\frac{\| (F^k_m)^e \|}{\| [k^e] \|}\right)^2 + \frac{4\, E^{ek}_{m+1}}{\| [k^e] \|}} \qquad (4.42)$$

such that here E^{ek}_{m+1} defines the constraint on the allowable local level energy excursion.

As can be seen from the above development, the bounds on the various field variables ultimately resulted in constraints on the levels of the $\Delta \underset{\sim}{Y}$ hierarchy of groups. This is directly due to the displacement type of FE formulation used to set up the governing equations.

The foregoing constraints have various advantages depending on structural geometry, material type, boundary, and loading conditions.

For instance, beam, plate and shell type thin walled structures undergo deformation processes which usually involve large deformation and slope changes when over loaded. Such behavior is typically well defined and thus, can be upper bounded for various loading conditions. Once the potential range of deflection and slope excursion are identified, the localized incremental constraints defined on nodal deformations and displacement gradients can be estimated. In this context, Δ_ℓ and ΔF_j can be obtained directly from design requirements and empirical data etc. This is incontrast to stress, strain and energy excursions which are less well defined in such structures. Regardless, as will be seen later, quite liberal constraints can be employed inconjunction with say the AHECS and still maintain stable and efficient iteration processes.

For thick walled structures which are dominated mainly by material nonlinearity (plasticity), the use of incremental stress, strain and energy excursion controls are more natural. This follows from the fact that formally, nonlinear constitutive relations are usually dependent on stress, strain and energy excursions.

Regardless of the approach taken, due to the use of the displacement type FE formulation, all the foregoing bounds eventually evolve into a displacement type constraint. In this context, the main thrust of the forthcoming benchmarking will be to document the numerical operating characteristics of displacement type localized bounds applied to the globally constrained INR. Here, special emphasis will be given to considering the AHECS type of scheme.

V. NUMERICAL BENCHMARKING

In the preceding sections, the constrained INR strategy was

modified to include several major improvements. These consist of:

i) The use of localized constraints to help automate/control and numerically stabilize the scheme and;

ii) The use of automatic abscissa/ordinate updating to enable the handling of problems which require either load, deflection or mixed load/deflection control.

To illustrate the improved convergence and efficiency characteristics of the modified constrained INR, the main thrust of this section will be to consider the results of several benchmark examples. Such benchmarks will attempt to:

i) Verify the schemes ability to handle highly nonlinear problems involving softening/hardening and buckling behavior along with inelastic/nonlinear material properties and;

ii) Carefully compare the scheme with the numerical properties of the MINR, FINR, and modified/BFGS updated INR and HECS algorithms.

Based on such goals, three benchmark examples are included for demonstration purposes namely:

i) The elastic buckling of a shallow arch;

ii) The elastic-plastic buckling of shallow arch;

iii) The load deflection characteristics of a shallow spherical cap.

The choice of the elastic shallow arch problem depicted in Fig. 5-1 follows from its turning point behavior which marks the transition between positive and indefinite stiffness behavior. The

elastic-plastic behavior of the arch was employed since plasticity greatly accentuates the nonlinearity/transitional behavior in the vicinity of buckling. Lastly, the spherical cap shown in Fig. 5-2 was considered since it possesses very shallow stiffness characteristics followed by strong stiffening. Such properties typically cause significant difficulties for unconstrained INR type schemes.

To implement such goals, the modified constrained INR strategy was introduced into the ADINA 77 FE code. This facilitated treatment of a wide variety of boundary conditions, material types, geometries and element families.

As was noted earlier, load stepping in a constrained scheme does not converge directly to the designated target values. To enable the handling of problems involving specific target loads/deflections, automatic ordinate/abscissa controls must be implemented in the constrained methodology. Table 5-1 illustrates a comparison of the targeting capabilities of the AHECS and HECS controlled INR. As can be seen, the AHECS converges to the specified load increment. This is in contrast to the straight HECS whose converged value depends on the intersection between the load deflection response and the type of constraint surface employed.

As the first benchmarking activity, we shall consider the capability of the so-called AHECS modified INR to handle specific target loading values. Of particular interest will be the evaluation of the new schemes stability inconjunction with its numerical efficiency.

For example, Tables 5.2 - 5.4 illustrate the load step sensitivity of the AHECS modified INR. As can be seen, with increasing load step size, the unconstrained scheme completely fails while the AHECS especially

with BFGS updating remains quite stable. Comparing the HECS with the AHECS, we see from Tables 5.3 and 5.4 that the number of required stiffness updates is significantly reduced with the use of automatic abscissa/ordinate adjustment.

Next, the ability to handle load stepping in the neighborhood of buckling will be considered. Noting the arch depicted in Fig. 5-1, Fig. 5-3 illustrates the load deflection characteristics of the centrally loaded case. In the context of Table 5.5, the inherent stability and efficiency of the AHECS to obtain the turning point is clearly illustrated. Again the BFGS updated version is numerically more efficient. This is especially true as load increment size increases.

Comparison of the handling characteristics in the elastic-plastic postbuckling range of arch behavior is given in Table 5.6. Based on the model employed, the progressive growth of plastic sites during collapse can be seen by noting the sequence defined by Figs. 5.4 and 5.5. Note the case considered consists of an arch wherein plasticization is initiated just prior to buckling. This is clearly illustrated in Fig. 5.4. Such a zone represents a relatively severe transition in behavior and hence a natural benchmark test. As seen from Table 5.6, a comparison of the various constraint schemes illustrates that the AHECS requires significantly less stiffness updates to yield numerically stable converged solution.

Noting the spherical cap given in Fig. 5.2, Fig. 5.6 illustrates its force deflection response to central loading. In the context of such system behavior, Table 5.7 depicts the efficiency of the AHECS over the straight HECS. Specifically, the AHECS required significantly less full stiffness updates to converge to the designated load level. This is

particularly true in the shallow range of cap behavior where numerous load steps are usually necessary.

We shall now consider the relative merits associated with the use of local constraints to automate load stepping. This will be approached from two points of view namely:

i) The use of local constraints to control stepsize so as to yield prescribed loads/displacements and;

ii) Defining the load/displacement increment sensitivity of the scheme.

For example in terms of the centrally loaded arch. Tables 5.8 - 5.11 illustrate the aspects denoted by i) and ii) given above. In particular, as can be seen from these tables, a wide range of load steps and local deflection constraints are stabily and efficiently accomodated by the scheme. Specifically, essentially unlimited load step sizes can be handled. In addition to illustrating sensitivity to load and local constraint step size, the results given in Tables 5.8 - 5.11 also point to the fact that localized constraints can be used to handle either load or deflection control. In particular, two target deflection states were considered in the postbuckling range namely .4 and .8 inches. These are illustrated in Fig. 5-7. As seen from the Tables, the results were essentially independent of step size. This is clearly illustrated by the fact that the number of iterations does not vary significantly, as step size increased. Again, the BFGS version has a decided advantage over the MINR type constrained scheme especially as the number of increments is increased.

The preceding developments and associated benchmarks have illustrated the wide ranging potentials/capabilities and numercal robustness

of the concept of using localized constraints to, resize and reshape the global constraint surface controlling successive iterations of the INR family of nonlinear FE solution algorithms. Due to their overall algorithmic structure, such procedures are easily adapted to use in general purpose FE computer codes.

VI. SUMMARY

As seen in the preceding section, this paper has developed numerical strategies which enable the automatic adjustment of load/deflection incrementation for NR type nonlinear FE equation solvers. This was achieved through the introduction of a hierarchy of localized constraints which enable the control/delimiting of the iterative excursions of the governing field variables. Such constraints enable the automatic adjustment of the size, shape, and orientation of the global constraint surface used to control the NR solver. As can be seen from the development, localized bounds can be established for any of the governing field variables. This includes the establishment of localized bounds on excursions in displacement, the deformation gradients stress, strain, as well as in energy.

Due to the generality of the approach taken, a wide variety of constraint surface geometries can be handled by the overall methodology. Note, such constraints have advantages which are dependent on structural configuration, material properties, as well as, on boundary and loading conditions. Specifically, deformation and deformation gradient control are better suited to thin walled structure. In contrast, for thick walled configurations, constraints on stress, strain and energy are more useful. For structure containing both thick and thin walled components,

a combination of localized constraints can be used to control the resizing, shaping and orientation process leading to automatic incrementation.

Due to the manner of formulation, the overall scheme can be incorporated in most general purpose FE codes. Such a process would require little rearchitecturing, especially if good data management procedures are in effect.

Overall, the project has resulted in numerous papers in a wide variety of national and international journals. These include:

1. Computers and Structures
2. Computational Mechanics
3. International Jr. of Engineering Science
4. Franklin Institute
5. Finite Elements in Analysis and Design
6. Engineering Mech. ASCLE
7. AIAA

A total list of papers is given in Appendix 3.

ACKNOWLEDGEMENT

The first author is grateful to Dr. C. Chamis of NASA Lewis for the stimulating discussions and encouragements during the course of the work. The second author expresses his appreciation to Dr. Jim Stafford of B. F. Goodrich for his support and encouragement.

REFERENCES

1. Wempner, G.A., "Discrete Approximations Related to Nonlinear Theories of Solids", Int. J. Solids Structures 7, 1581 (1971).

2. Riks, E., "An Incremental Approach to the Solution of Snapping and Buckling Problems", Int. J. Solids Structures 15, 529 (1979).

3. Crisfield, M.A., "A Fast Incremental/Iterative Procedure That Handles Snapthrough", Comput. Structures 13, 55 (1981).

4. Padovan, J. and S. Tovichakchaikul, "Self-adaptive Predictor-Corrector Algorithms for Static Nonlinear Structural Analysis". Comput. Structures 15, 365 (1982).

5. Padovan, J. and T. Arechaga, "Formal Convergence Characteristics of Elliptically Constrained Incremental Newton-Raphson Algorithms" Int. J. Engrg. Sci. 20, 1077 (1982).

6. Padovan, J., S. Tovichakchaikul and T. Arechaga, "Operating Characteristics of Hyperbolically and Elliptically Constrained Self-adaptive Incremental Newton-Raphson Algorithms, J. Franklin Inst. 316, 197 (1983).

7. Padovan, J. and S. Tovichakchaikul, "Algorithms for Elastic-plastic-creep Postbuckling", Jr. of Engrg. Mech. ASCE, Vol. 110, pp. 911, (1984)

8. Matthies, H. and G. Strang, "The Solution of Nonlinear Finite Element Equations", Int. J. Num. Meth. Engrg. 14, 1612 (1979).

9. Bathe, K.J. and A.P. Cimento, "Some Practical Problems for the Solution of Nonlinear Finite Element Equations" Comp. Meth. Appl. Mech. Engrg. 22, 59 (1980).

10. Padovan, J. and S. Tovichakchaikul, "Pseudoupdated Constrained Solution Algorithm for Nonlinear Heat Conduction", AIAA Jr., Vol 21, pp 902, (1983).

11. Padovan, J., "Self-adaptive Incremental Newton-Raphson Algorithms", NASA CP-2147, pp 115, (1980).

12. Ortega, J.M., and W.C. Rheinboldt, "Iterative Solution of Nonlinear Equations in Several Variables", Academic Press, New York, (1970).

13. Fung, Y.C, "Foundations of Solid Mechanics", Prentice Hall, Englewood Cliffs, New Jersey (1965).

14. Zienkieweicz, O.C., "The Finite Element Method", McGraw-Hill, New York (1977).

15. Bathe, K.J., "Finite Element Procedures in Engineering Anaiysis", Prentice Hall, Engelwood Cliffs, New Jersey (1982).

FIGURE AND TABLE CAPTIONS

Figure No.	Caption
2.1	Intersection of INR type stiffness extrapolation of solution curve and $\underline{F}$ = constant constraint curve in force deflection space
2.2	INR type iterations/extrapolations bound by oblique linear, circular elliptic and piecewise continuous hyperbolic constraint curves
2.3	Elliptically constrained INR iterations about buckling point
2.4	Typical failures of oblique linear, circular, elliptic and piecewise hyperbolic constraint surfaces due to "mis-sizing"
2.5	Load step utilization of various constrained INR methodologies
3.1	Rotated and rotated-translated hyperplanar constraint
3.2	Iteration process associated with translated hyperbolic constraint
3.3	Iteration process associated with abscissa stretched HECS
3.4	Targeting oblique linear constraint curve via sweeping through fixed angular increments
3.5	Targeting oblique linear constraint curve via sweeping through fixed force increments
3.6	Targeting oblique linear constraint curve via sweeping through fixed MINR estimated ΔY

Applied Load Step ΔF	HECS (MINR, BFGS)	AHECS (MINR, BFGS)
15 lb	10.35 lb	15 lb
25 lb	16.25 lb	25 lb
30 lb	19.2 lb	30 lb

Table 5.1 Comparison of Single Step Converged Final Solution Values for Centrally Loaded Arch

Applied Load Step lb.	FINR Iter.	MINR Iter.	AHECS (MINR) Iter.	AHECS (BFGS) Iter.
2	2	3	5	4
5	3	5	6	5
10	3	7	8	5
15	4	9	9	5
25	Failed	Failed	12	6
30	Failed	Failed	17	6

Table 5.2 Load Step Sensitivities of FINR, MINR, MINR-AHECS and BFGS-AHECS

Load Steps (lb)		2	5	10	15	30
MINR-HECS	Final Load (lb)	30.9	29.5	31.1	31.1	30.9
	Updates/Iter. (Total)	$\frac{23}{31}$	$\frac{16}{25}$	$\frac{10}{21}$	$\frac{7}{17}$	$\frac{5}{11}$
MINR-AHECS	Final Load (lb)	30	30	30	30	30
	Updates/Iter. (Total)	$\frac{15}{43}$	$\frac{6}{31}$	$\frac{3}{27}$	$\frac{2}{22}$	$\frac{1}{15}$

Table 5.3 Stiffness Update/Iteration Requirements for MINR Modified HECS and AHECS Algorithms: Arch Subject to 30 lb Target

LOAD STEPS (lb)		2	5	10	15	30
BFGS-HECS	Final Load (lb)	30.9	29.5	31.1	31.1	30.9
	Updates/Iter. (Total)	$\frac{23}{31}$	$\frac{16}{25}$	$\frac{10}{21}$	$\frac{7}{15}$	$\frac{5}{7}$
BFGS-AHECS	Final Load (lb)	30	30	30	30	30
	Updates/Iter. (Total)	$\frac{15}{23}$	$\frac{6}{17}$	$\frac{3}{14}$	$\frac{2}{9}$	$\frac{1}{4}$

Table 5.4 Stiffness Update/Iteration Requirements for BFGS Modified HECS and AHECS Algorithms: Arch Subject to 30 lb Target Load

Applied Load Step (lb)	2	5	10	15	25	30
Full INR	Failed	Failed	Failed	Failed	Failed	0
MINR	Failed	Failed	Failed	Failed	Failed	0
MINR-HECS	$\frac{71}{77}$	$\frac{29}{45}$	$\frac{15}{38}$	$\frac{7}{29}$	$\frac{6}{20}$	$\frac{5}{13}$
BFGS-HECS	$\frac{71}{76}$	$\frac{29}{44}$	$\frac{14}{33}$	$\frac{7}{22}$	$\frac{6}{16}$	$\frac{4}{9}$
MINR-AHECS	$\frac{43}{102}$	$\frac{24}{54}$	$\frac{10}{45}$	$\frac{5}{32}$	$\frac{4}{26}$	$\frac{3}{21}$
BFGS-AHECS	$\frac{43}{95}$	$\frac{16}{47}$	$\frac{11}{30}$	$\frac{5}{17}$	$\frac{4}{12}$	$\frac{2}{6}$

Table 5.5 Stiffness Update/Iteration Requirements to Calculate Buckling Point of Centrally Loaded Arch

Applied Load Step (lb)	.5	1.	2.
MINR-HECS	$\frac{75}{91}$	$\frac{68}{79}$	$\frac{48}{54}$
BFGS-HECS	$\frac{75}{91}$	$\frac{68}{78}$	$\frac{48}{53}$
MINR-AHECS	$\frac{51}{110}$	$\frac{41}{91}$	$\frac{30}{70}$
BFGS-AHECS	$\frac{51}{110}$	$\frac{41}{83}$	$\frac{30}{61}$

Table 5.6 Stiffness Update/Iteration Requirements to Calculate Elastic-Plastic Postbuckling Behavior of Arch (Fig. 5.4)

Applied Load Step (lb)		1.0	5.0
BFGS-HECS	Final Load (lb)	30.02	30.76
	Updates/Iter. (Total)	$\frac{138}{145}$	$\frac{41}{23}$
BFGS-AHECS	Final Load (lb)	30	30
	Updates/Iter. (Total)	$\frac{30}{149}$	$\frac{6}{25}$

Table 5.7 Stiffness Update/Iteration Requirements for Cap Subject to 30 lb Target Load

No. of Load Steps	5	10	25	50	100
Load Step (lb)	100	100	100	100	100
δ_{crit} (in)	.08	.04	.016	.004	.008
Final Load Step (lb)	36.3	36.3	36.3	36.3	36.3
Final Deflection (in)	.4	.4	.4	.4	.4
MINR-HECS (Iter)	130	95	85	80	115
BFGS-HECS (Iter)	72	82	74	69	106

Table 5.8 Comparison of Efficiencies of Locally Constrained MINR-HECS and BFGS-HECS for Arch With .4 Inch Designated Target Deflection and 100 lb ΔF

No. of Load Steps	5	10	25	50	100
Load Step (lb)	500	500	500	500	500
δ_{crit} (in)	.08	.04	.016	.008	.004
Final Load Step (lb)	36.3	36.3	36.3	36.3	36.3
Final Deflection (in)	.4	.4	.4	.4	.4
MNR-HECS (Iter)	141	110	99	91	129
BFGS-HECS (Iter)	78	96	86	79	117

Table 5.9 Comparison of Efficiencies of Locally Constrained MINR-HECS and BFGS-HECS for Arch With .4 Inch Designated Target Deflection and 500 lb ΔF

No. of Load Steps	5	10	25	50	100
Load Step (lb)	100	100	100	100	100
δ_{crit} (in)	.16	.08	.032	.016	.008
Final Load Step (lb)	28.6	28.6	28.6	28.6	28.6
Final Deflection (in)	.8	.8	.8	.8	.8
MINR-HECS (Iter)	180	152	131	128	148
BFGS-HECS (Iter)	90	123	119	112	119

Table 5.10 Comparison of Efficiencies of Locally Constrained MINR-HECS and BFGS-HECS for Arch with .8m Designated Target Deflection and 100 lb ΔF

No. of Load Steps	5	10	25	50	100
Load Step (lb)	500	500	500	500	500
δ_{crit} (in)	.16	.08	.032	.016	.008
Final Load Step (lb)	28.6	28.6	28.6	28.6	28.6
Final Deflection (in)	.8	.8	.8	.8	.8
MNR-HECS (Iter)	191	162	141	139	157
MNR-HECS (Iter)	92	138	121	119	125

Table 5.11 Comparison of Efficiencies of Locally Constrained MINR-HECS and BFGS-HECS for Arch With .8m Designated Target Deflection and 500 lb ΔF

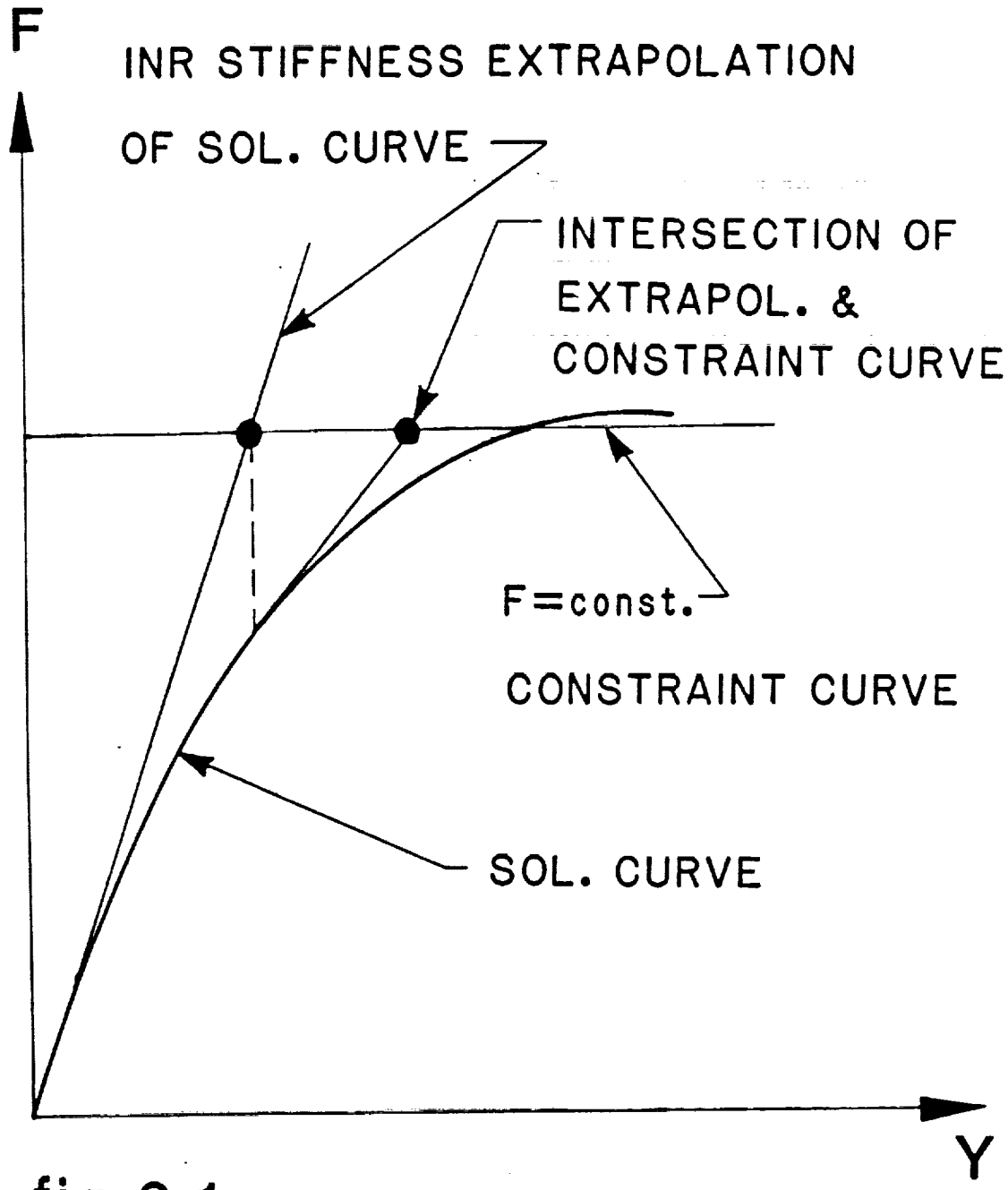
F
INR STIFFNESS EXTRAPOLATION
OF SOL. CURVE
INTERSECTION OF
EXTRAPOL. &
CONSTRAINT CURVE
F=const.
CONSTRAINT CURVE
SOL. CURVE
Y

fig 2.1

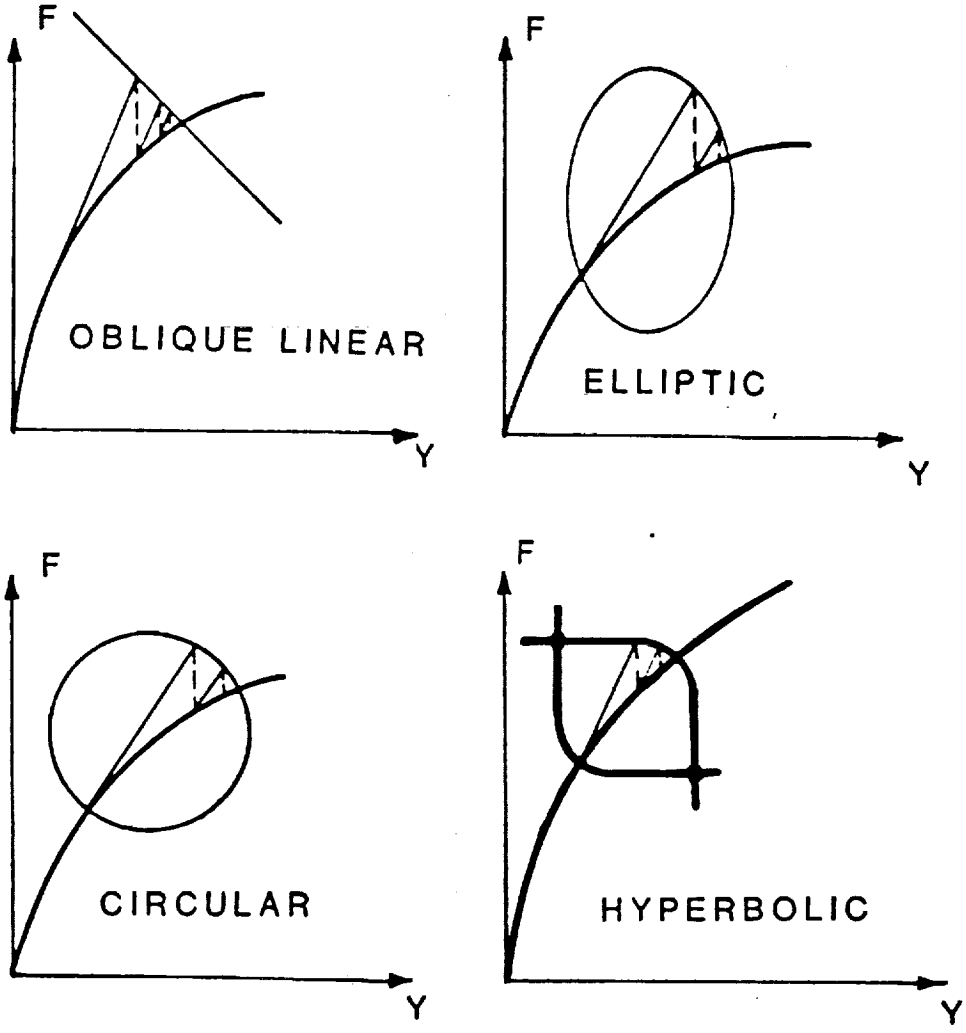

fig 2.2

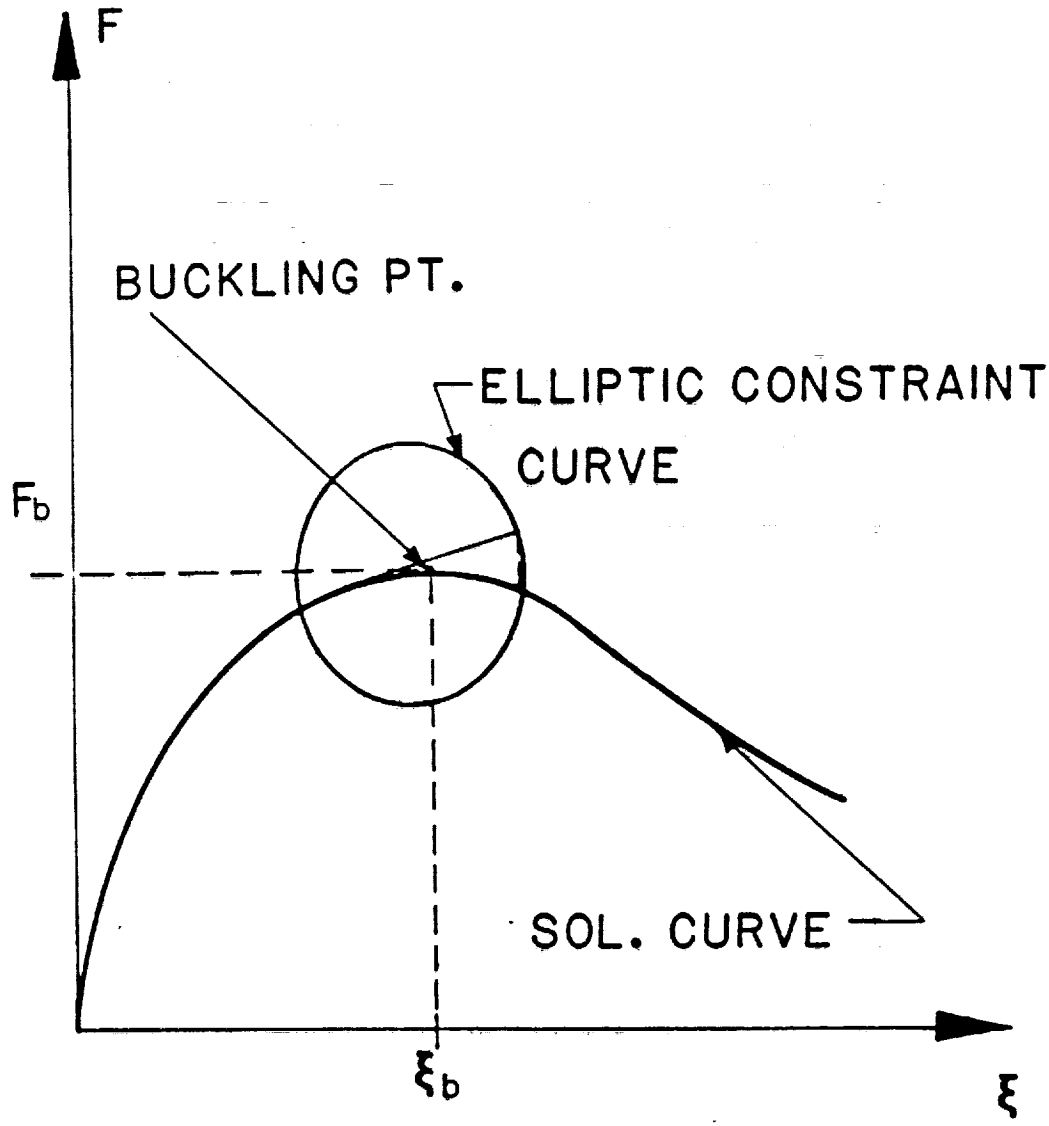

fig 2.3

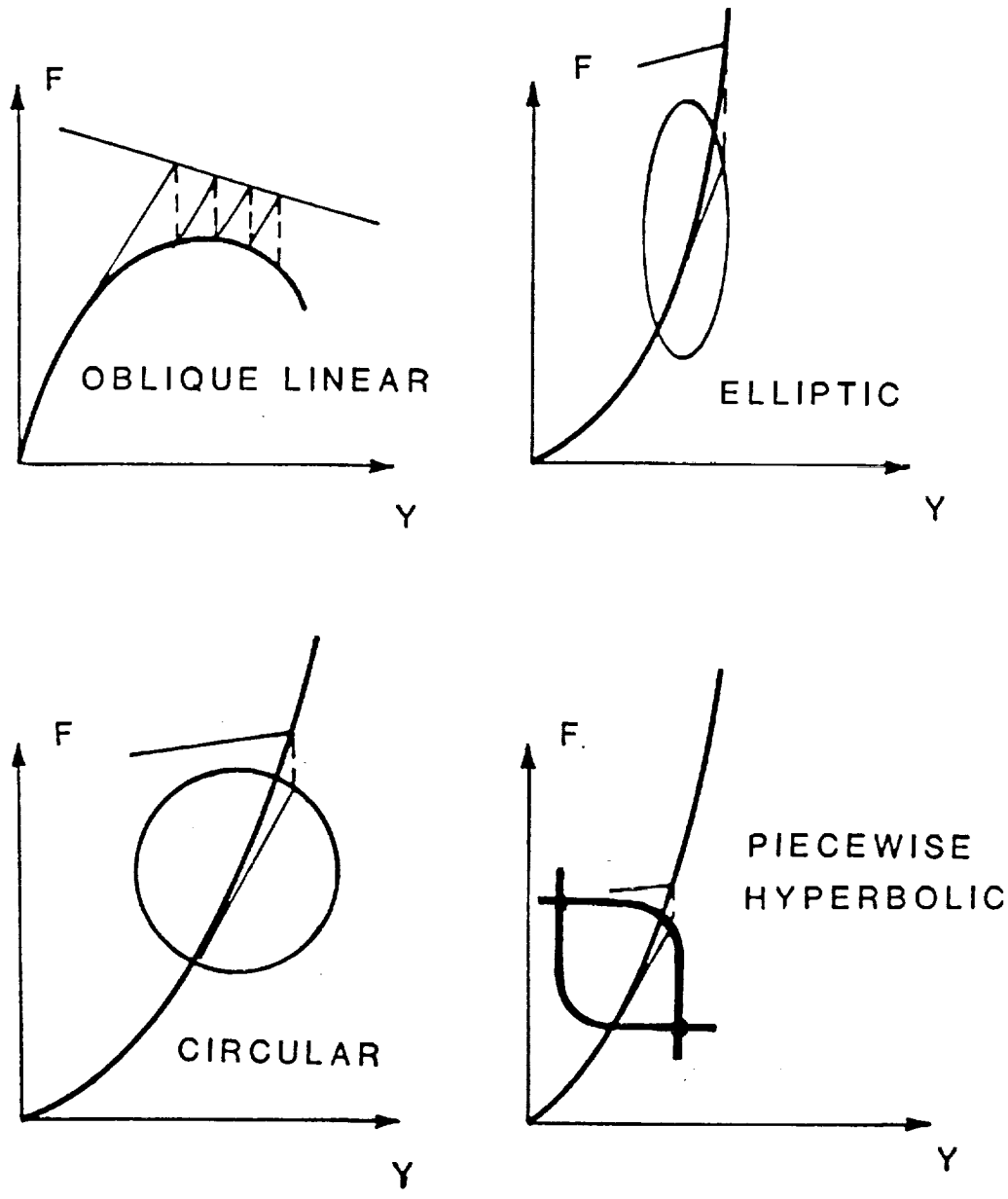
F
OBLIQUE LINEAR
Y
F
ELLIPTIC
Y
F
CIRCULAR
Y
F
PIECEWISE
HYPERBOLIC
Y

fig 2.4

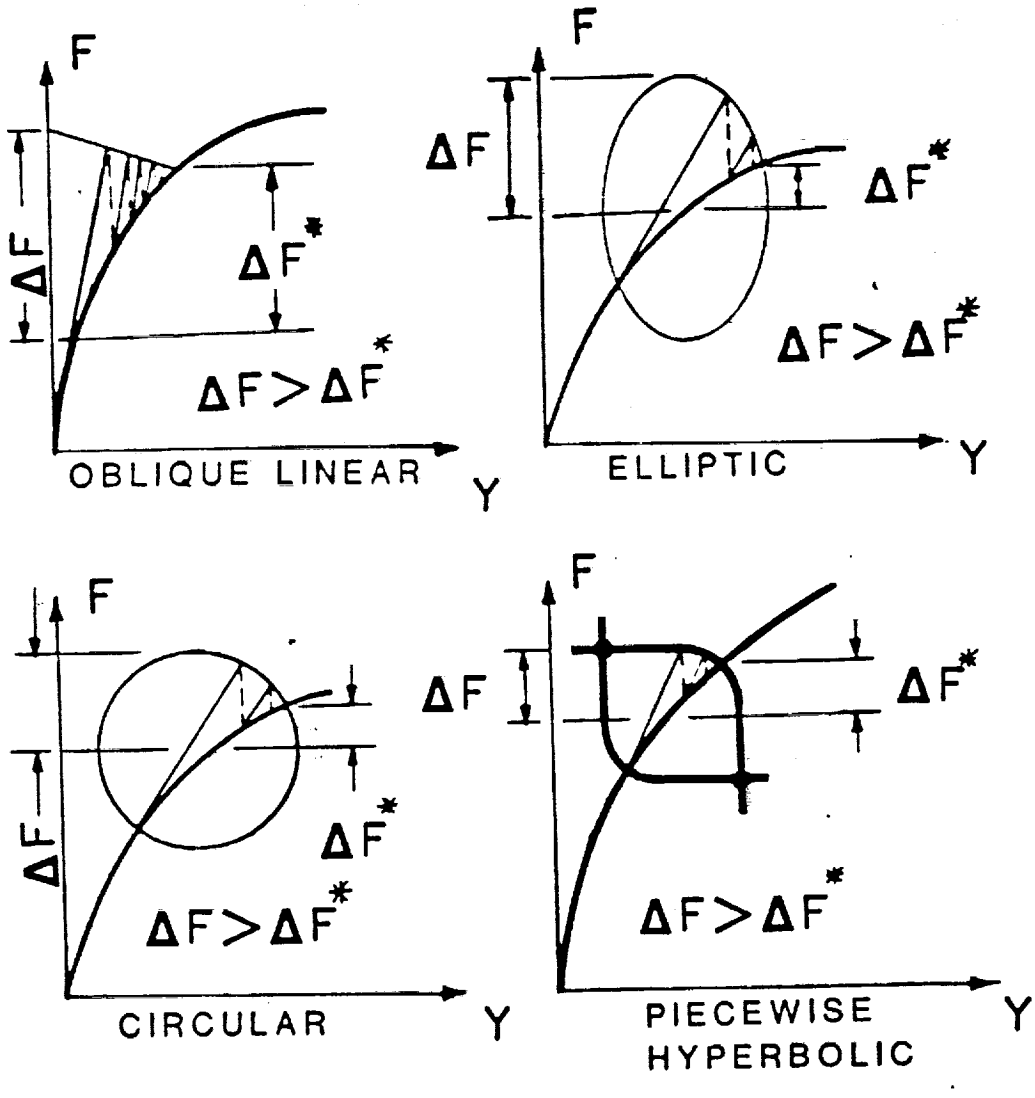
F
ΔF
ΔF*
ΔF>ΔF*
OBLIQUE LINEAR
Y
F
ΔF
ΔF*
ΔF>ΔF*
ELLIPTIC
Y
F
ΔF
ΔF*
ΔF>ΔF*
CIRCULAR
Y
F
ΔF
ΔF*
ΔF>ΔF*
PIECEWISE
HYPERBOLIC
Y

fig 2.5

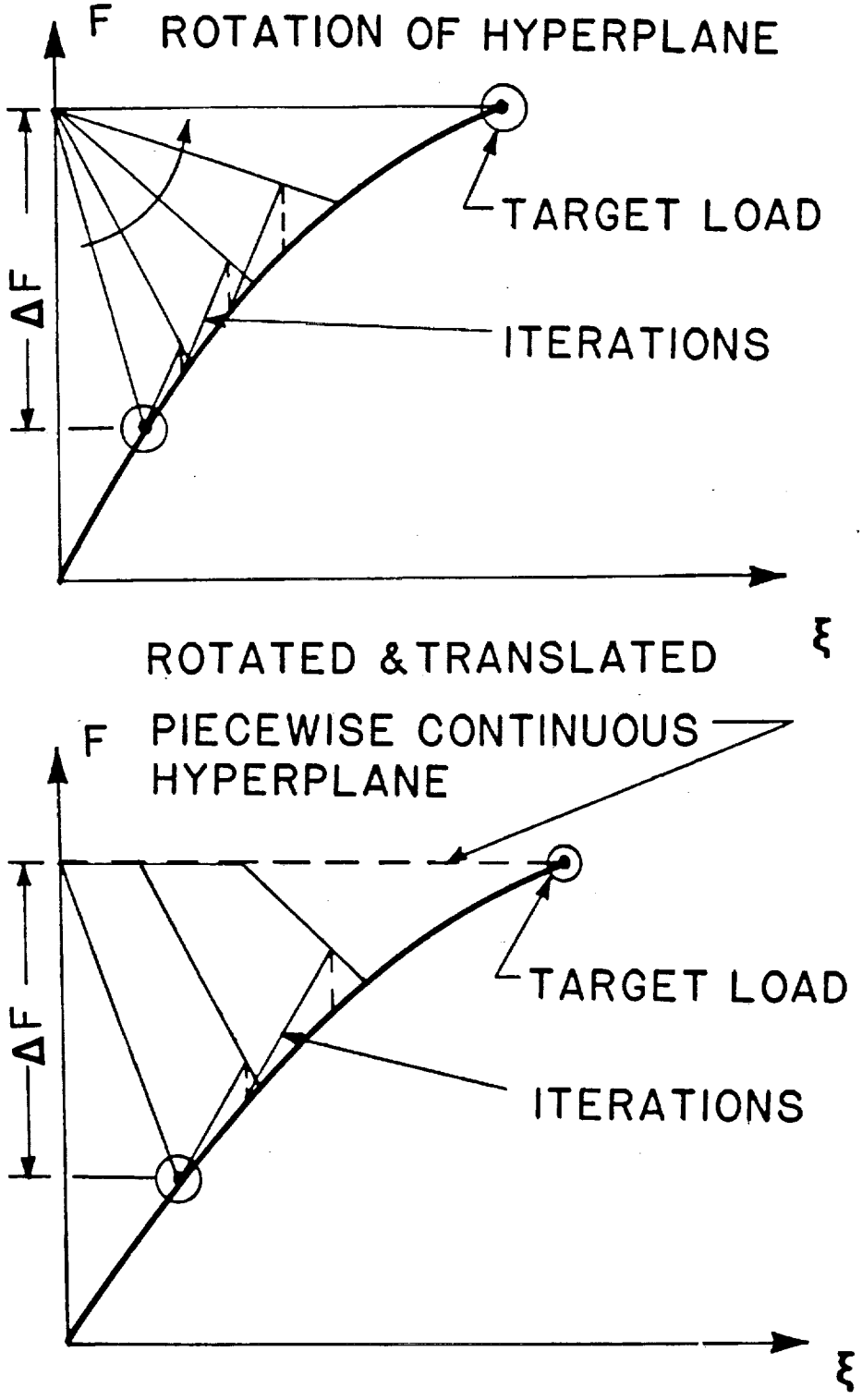
F
ROTATION OF HYPERPLANE
TARGET LOAD
ITERATIONS
ΔF
ξ
ROTATED & TRANSLATED
F
PIECEWISE CONTINUOUS HYPERPLANE
TARGET LOAD
ITERATIONS
ΔF
ξ

fig 3.1

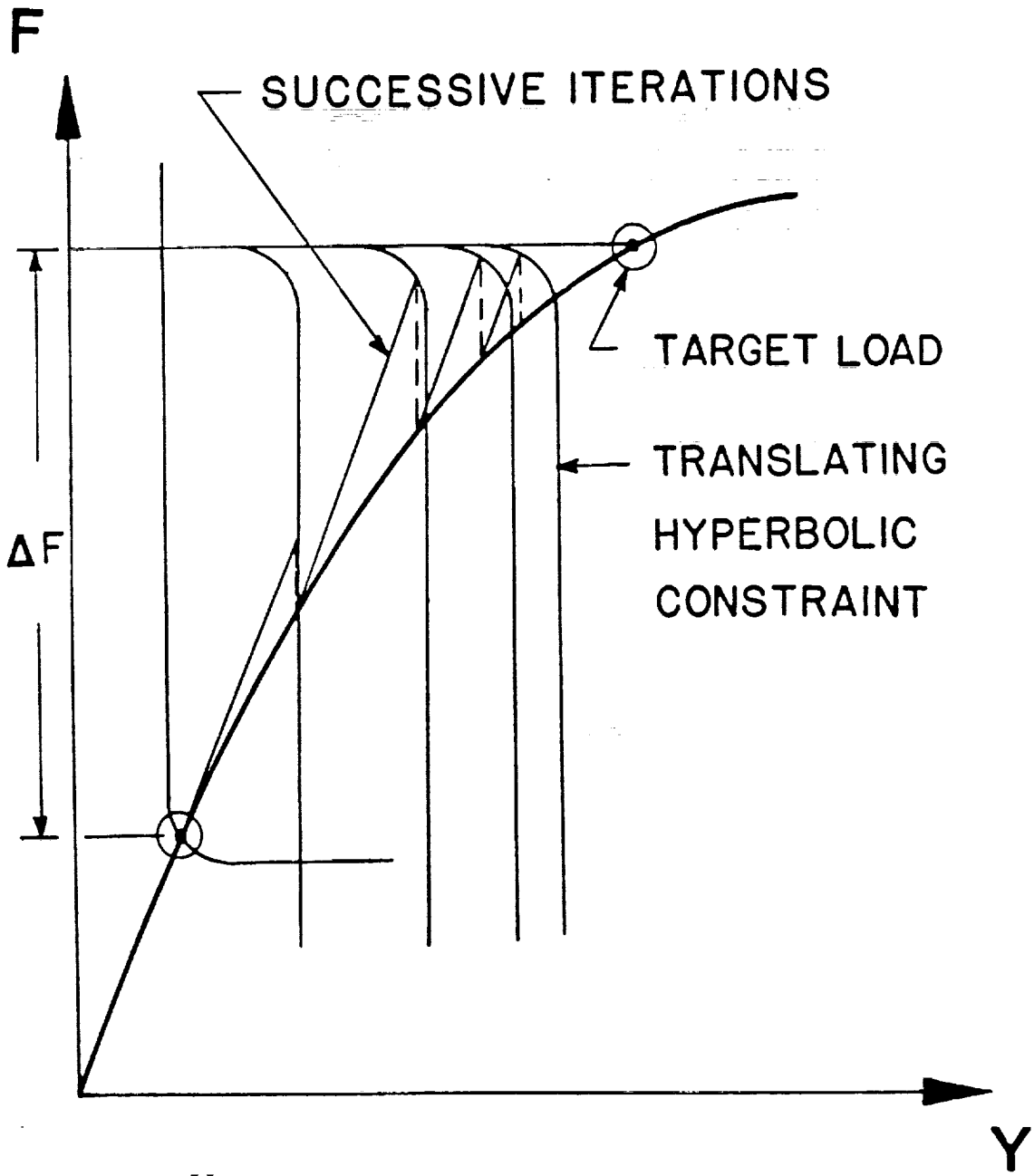
F
SUCCESSIVE ITERATIONS
TARGET LOAD
TRANSLATING
HYPERBOLIC
CONSTRAINT
ΔF
Y

fig 3.2

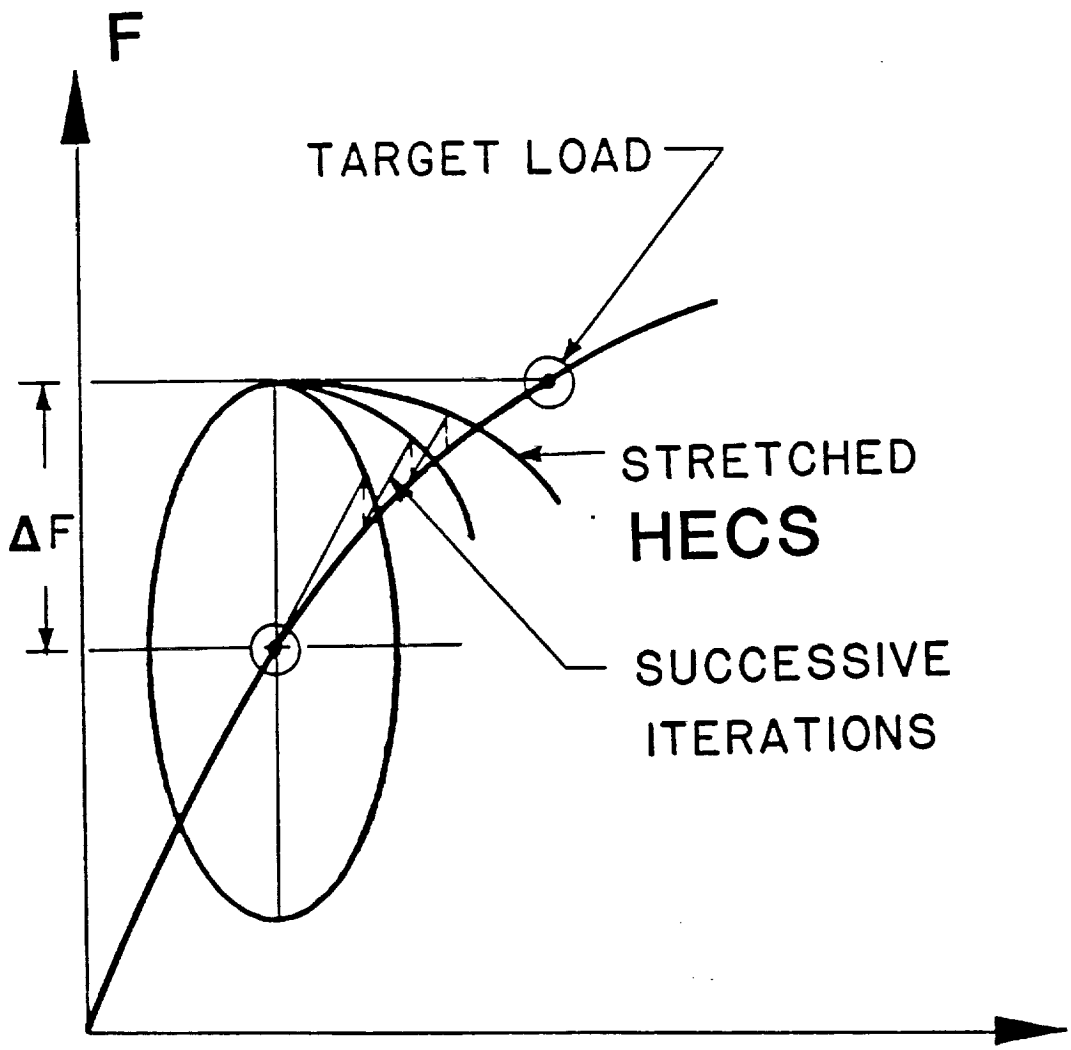

fig 3.3

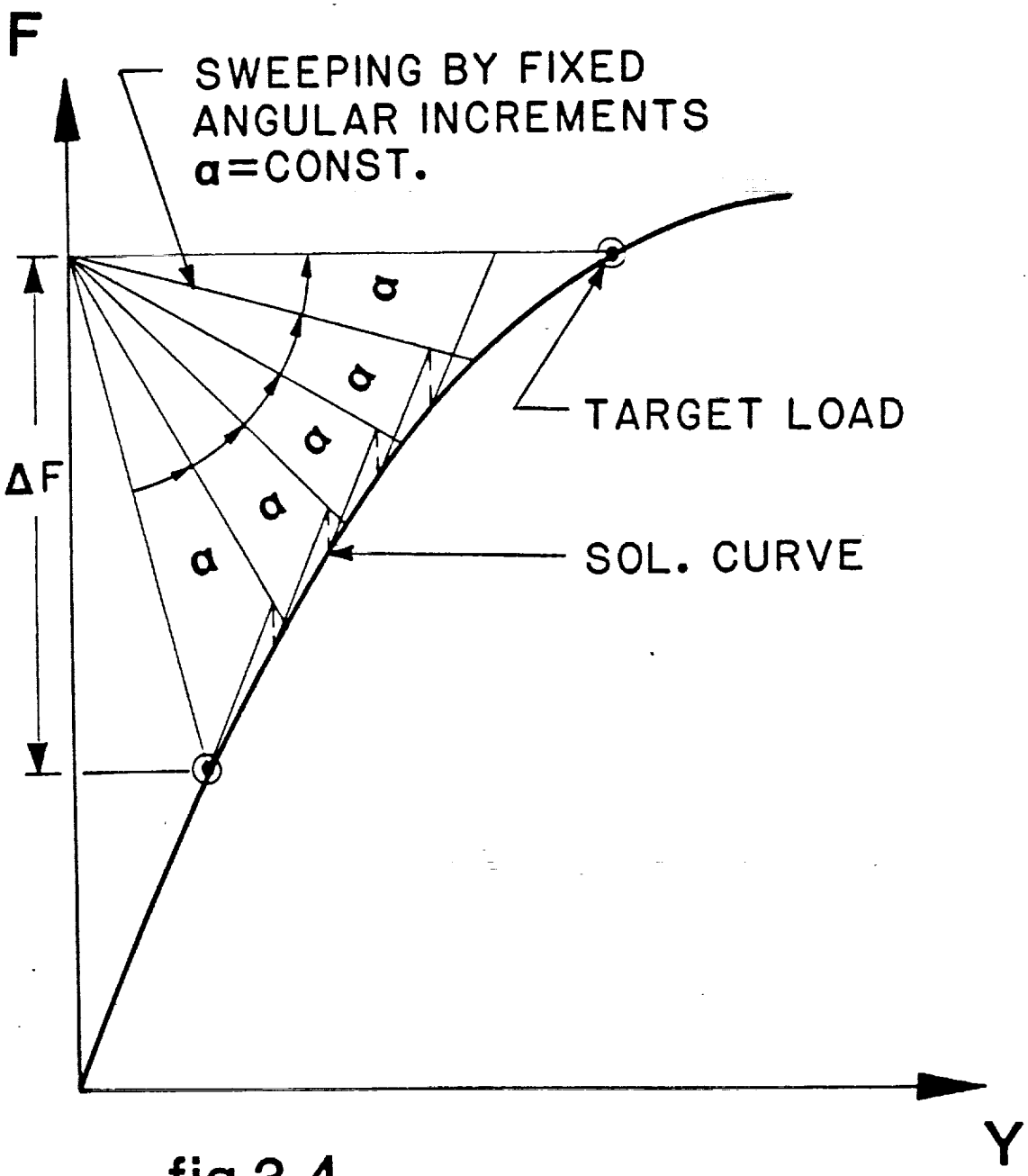
F
SWEEPING BY FIXED
ANGULAR INCREMENTS
α=CONST.
α
α
α
α
α
TARGET LOAD
SOL. CURVE
ΔF
Y

fig 3.4

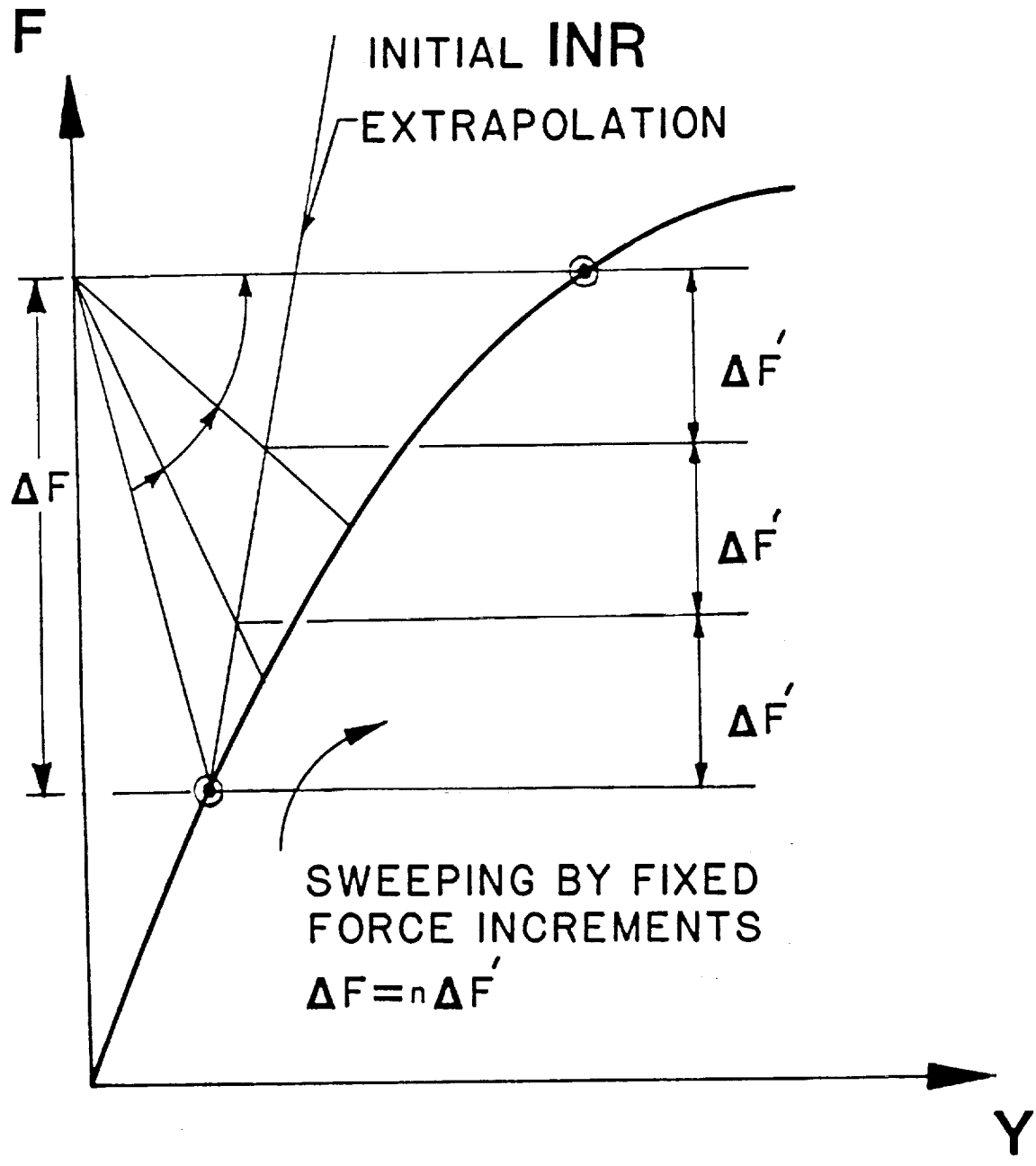
F
INITIAL INR
EXTRAPOLATION
ΔF
ΔF′
ΔF′
ΔF′
SWEEPING BY FIXED
FORCE INCREMENTS
ΔF=nΔF′
Y

fig 3.5

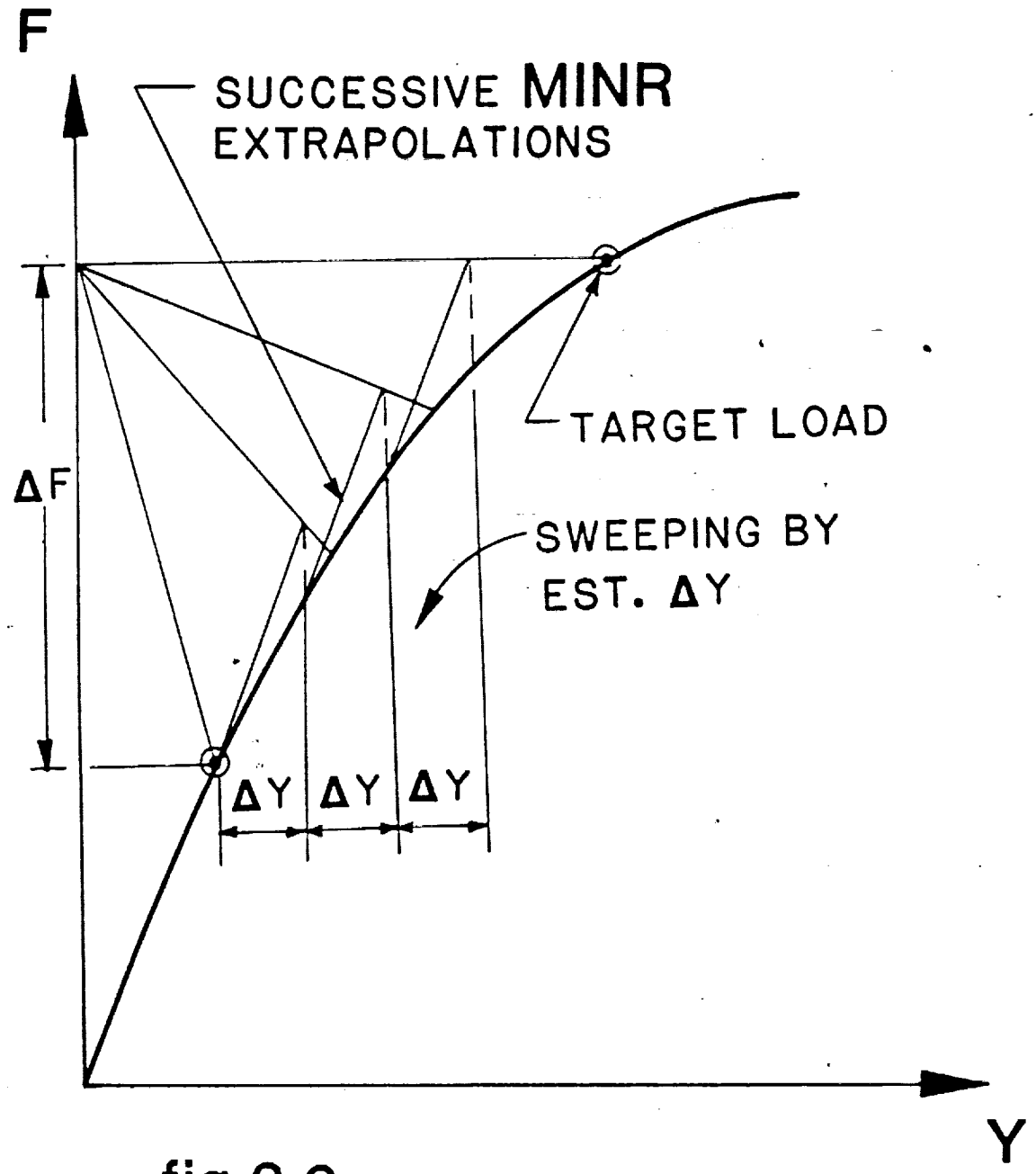
F
SUCCESSIVE MINR
EXTRAPOLATIONS
TARGET LOAD
ΔF
SWEEPING BY
EST. ΔY
ΔY
ΔY
ΔY
Y

fig 3.6

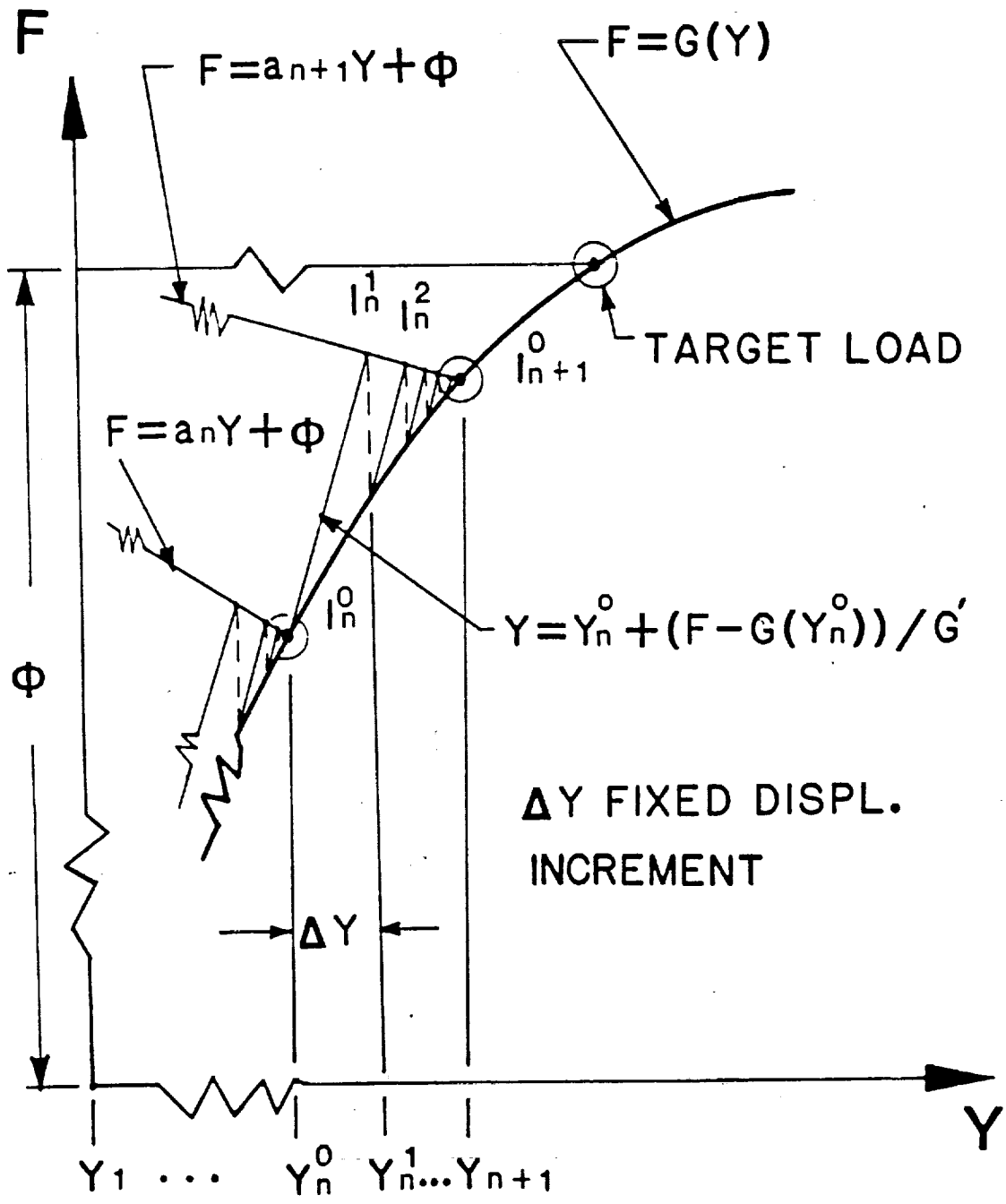
F
F=a n+1 Y+Φ
F=G(Y)
I n 1 I n 2
I n+1 0
TARGET LOAD
F=a nY+Φ
I n 0
Y=Y n 0 +(F−G(Y n 0))/G'
Φ
ΔY FIXED DISPL.
INCREMENT
ΔY
Y
Y 1 ... Y n 0 Y n 1 ... Y n+1

fig 3.7

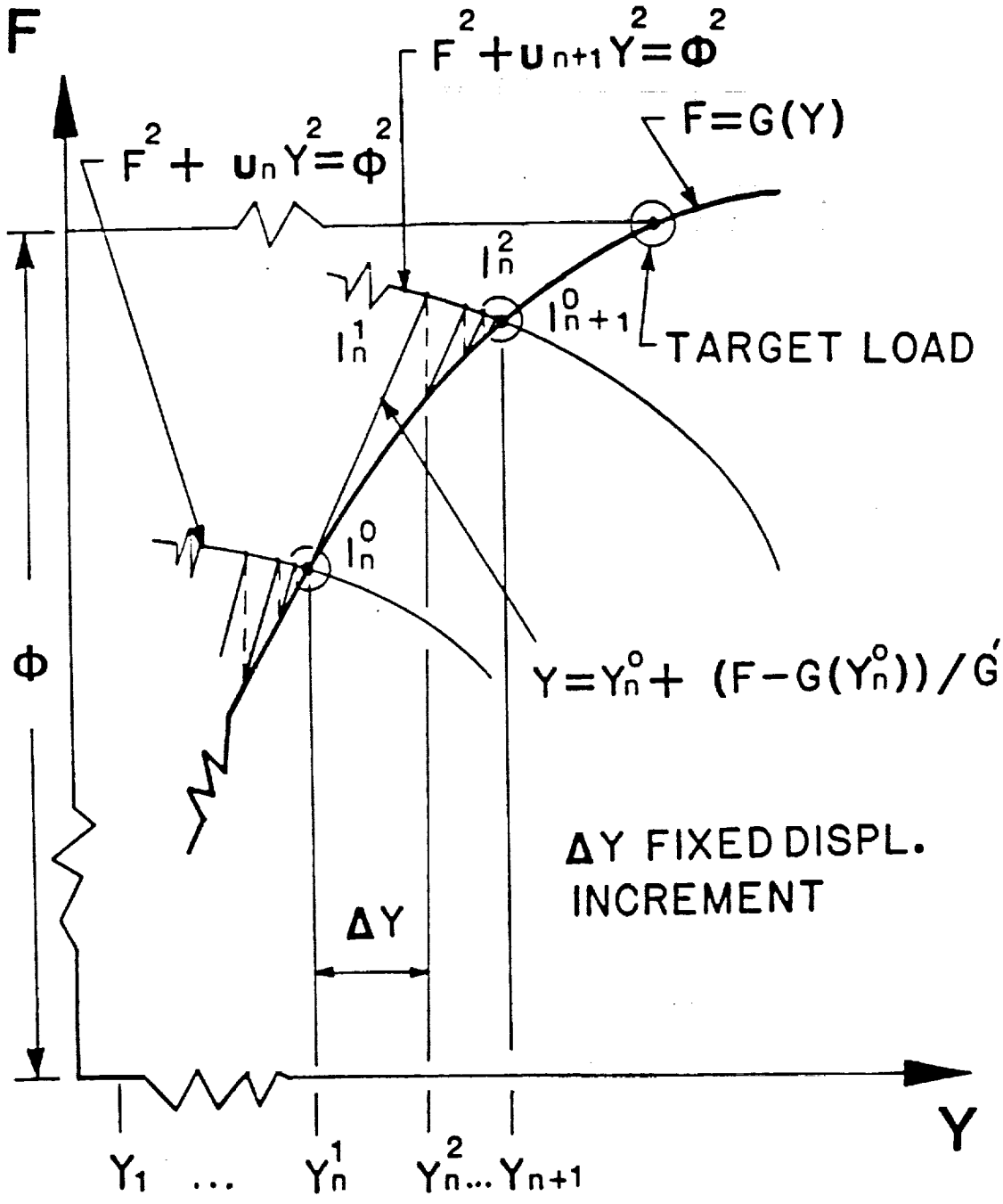
F
$F^2 + u_{n+1} Y^2 = \Phi^2$
$F^2 + u_n Y^2 = \Phi^2$
F=G(Y)
I_n^2
I_{n+1}^0
I_n^1
TARGET LOAD
I_n^0
Φ
$Y = Y_n^0 + (F - G(Y_n^0))/G'$
ΔY FIXED DISPL. INCREMENT
ΔY
Y
Y_1 ... Y_n^1 Y_n^2... Y_{n+1}

fig 3.8

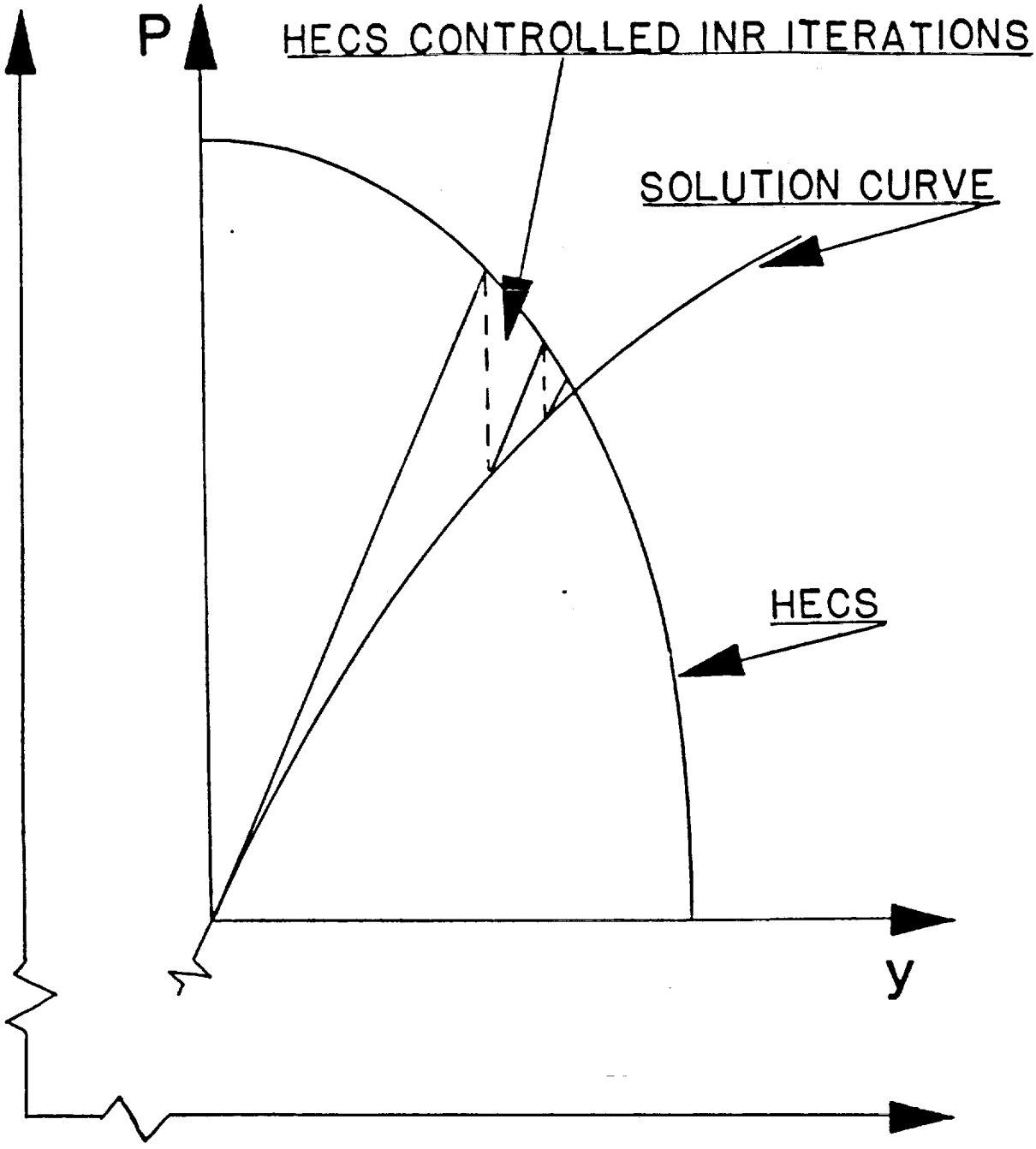

fig 4.1

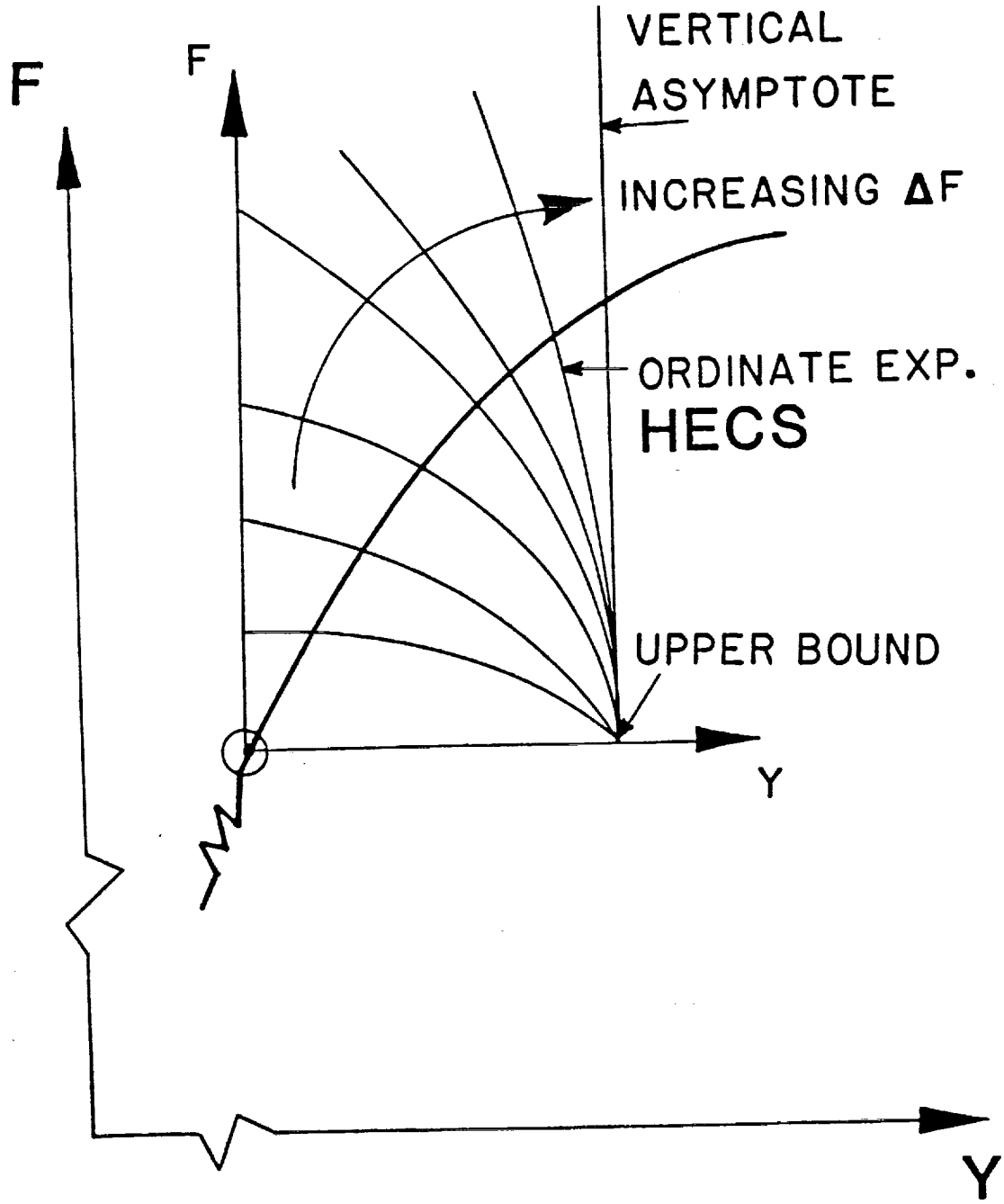
F
F
VERTICAL
ASYMPTOTE
INCREASING ΔF
ORDINATE EXP.
HECS
UPPER BOUND
Y
Y

fig 4.2

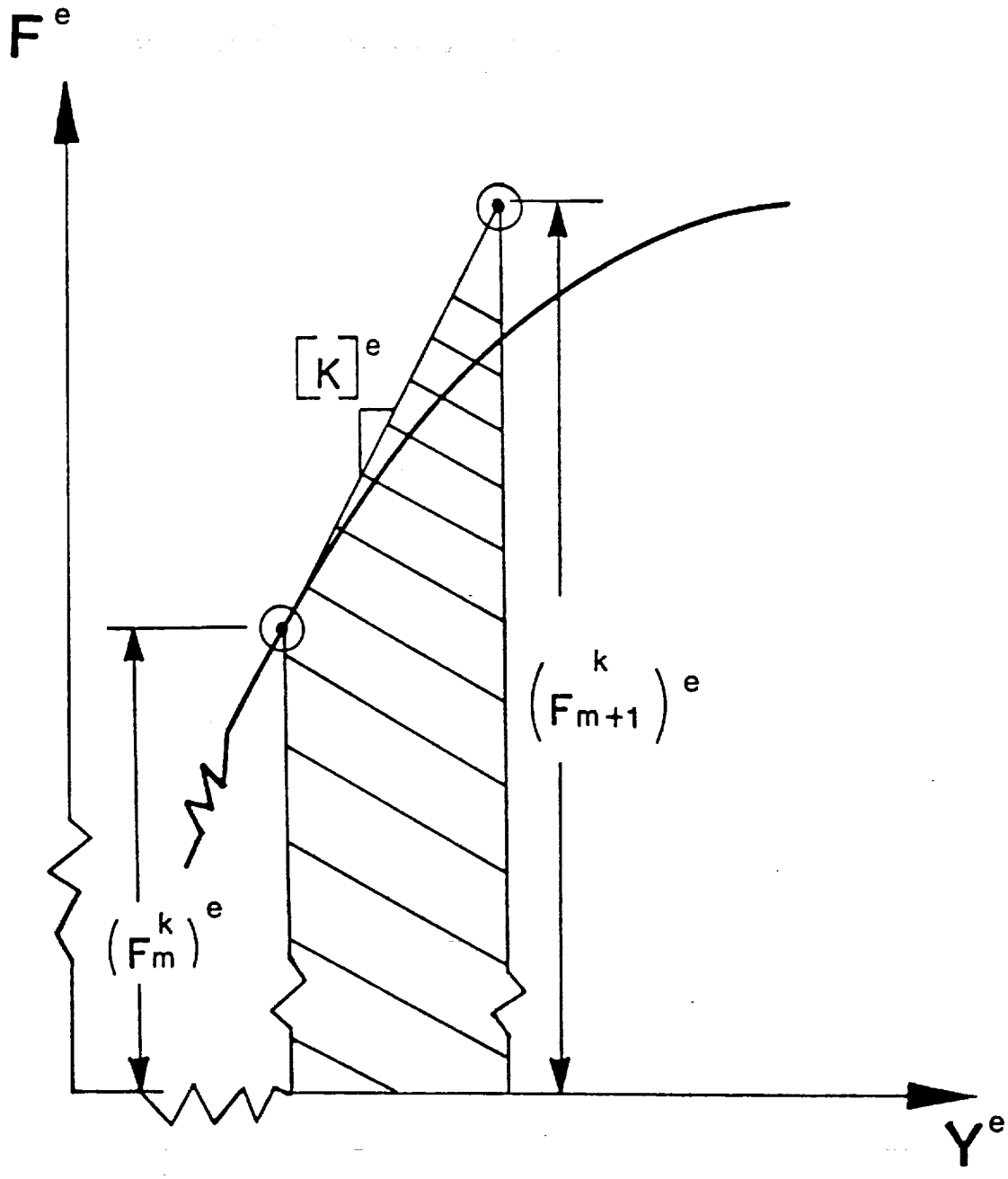

fig 4.3

2 D – 8 NODE ELEMENTS
PLANE STRESS

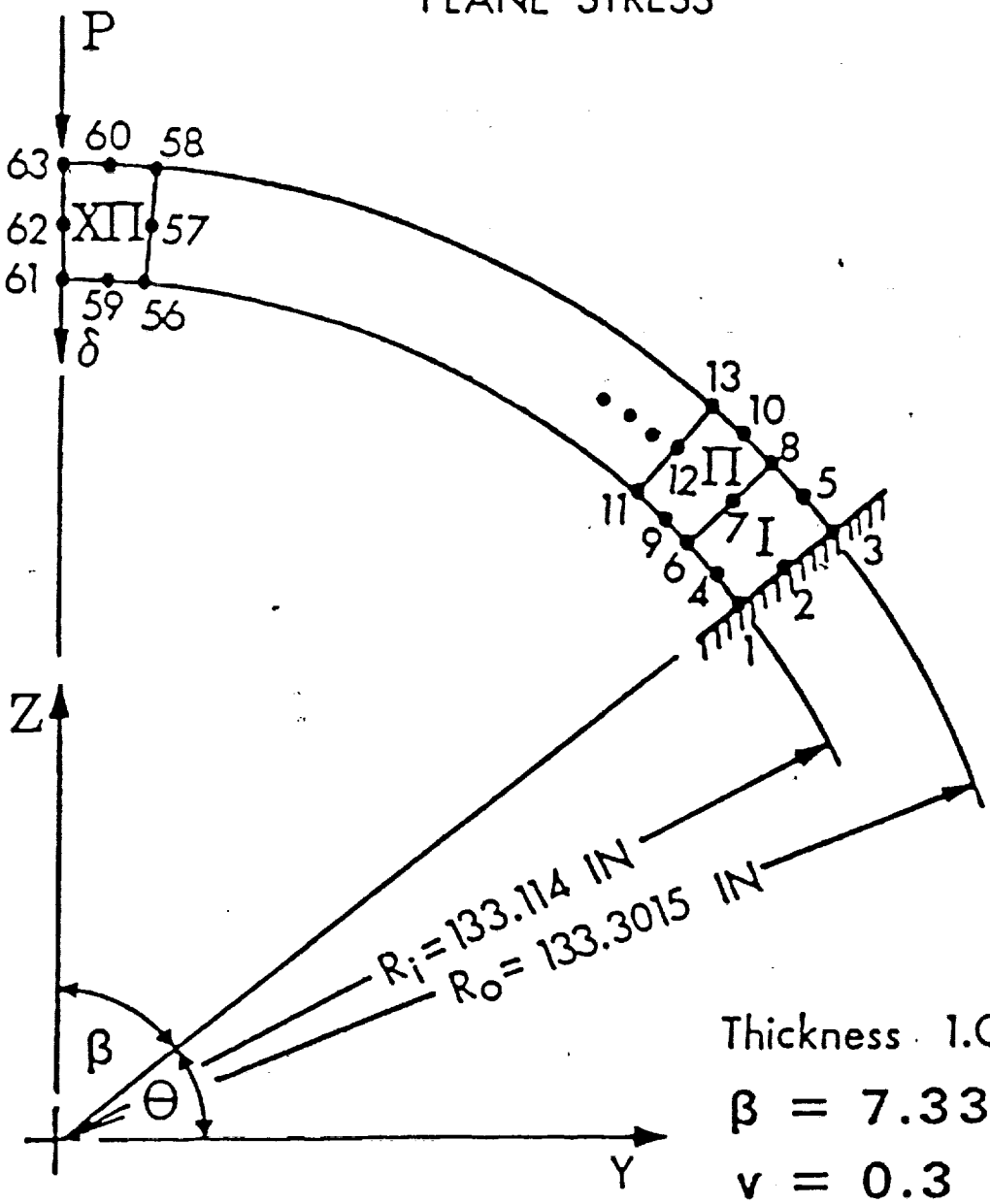

Thickness 1.0 in

$\beta = 7.3397°$

$\nu = 0.3$

$E = 1.0 \times 10^7$ PSI

$E_p = 0.$

$\sigma_y = 12.0$ ksi

fig 5.1

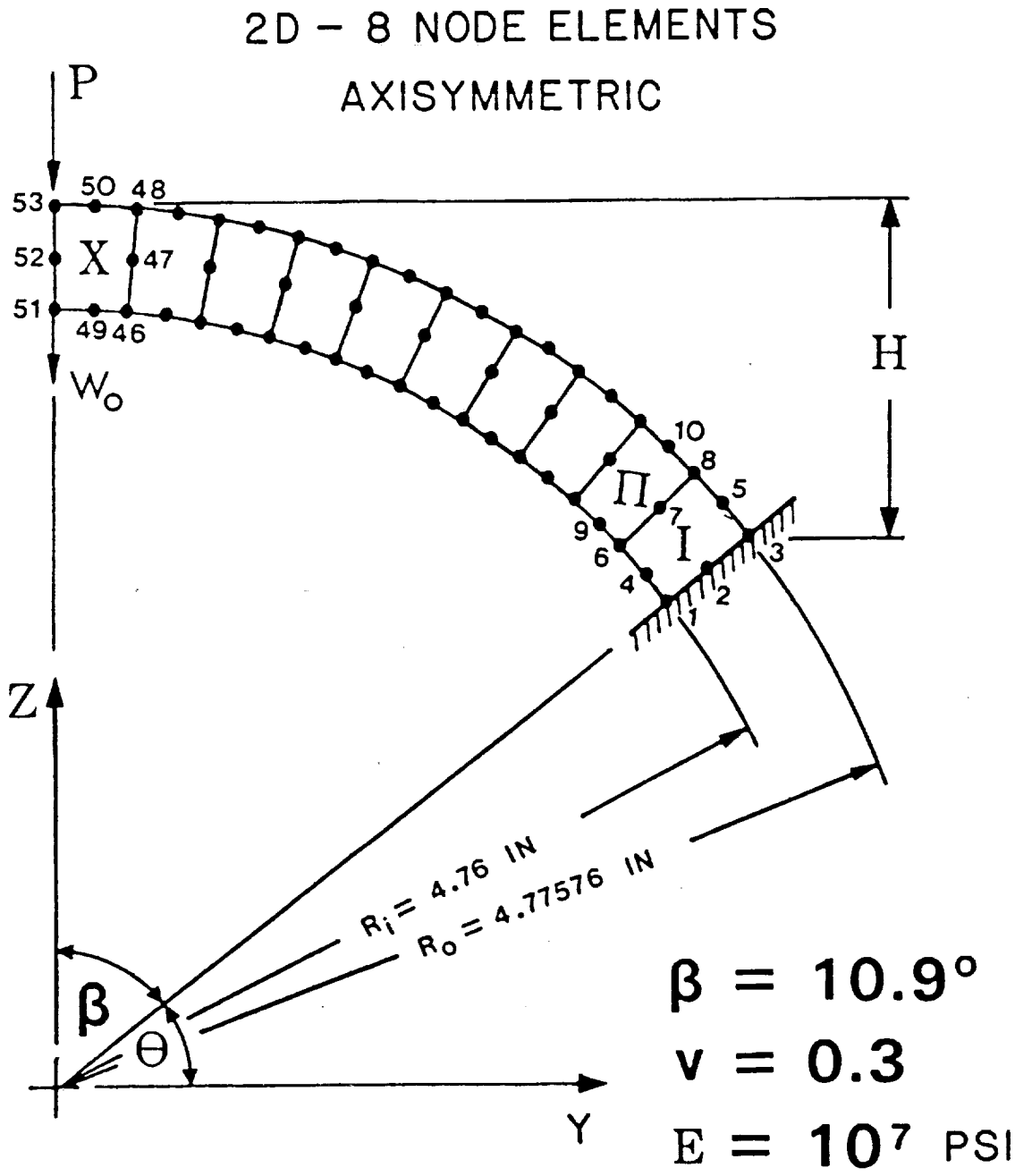
2D – 8 NODE ELEMENTS
AXISYMMETRIC
P
53
50
48
52
X
47
51
49
46
W_o
H
10
8
5
Π
9
7
I
6
3
4
2
1
Z
R_i = 4.76 IN
R_o = 4.77576 IN
β
θ
Y
β = 10.9°
v = 0.3
E = 10^7 PSI

fig 5.2

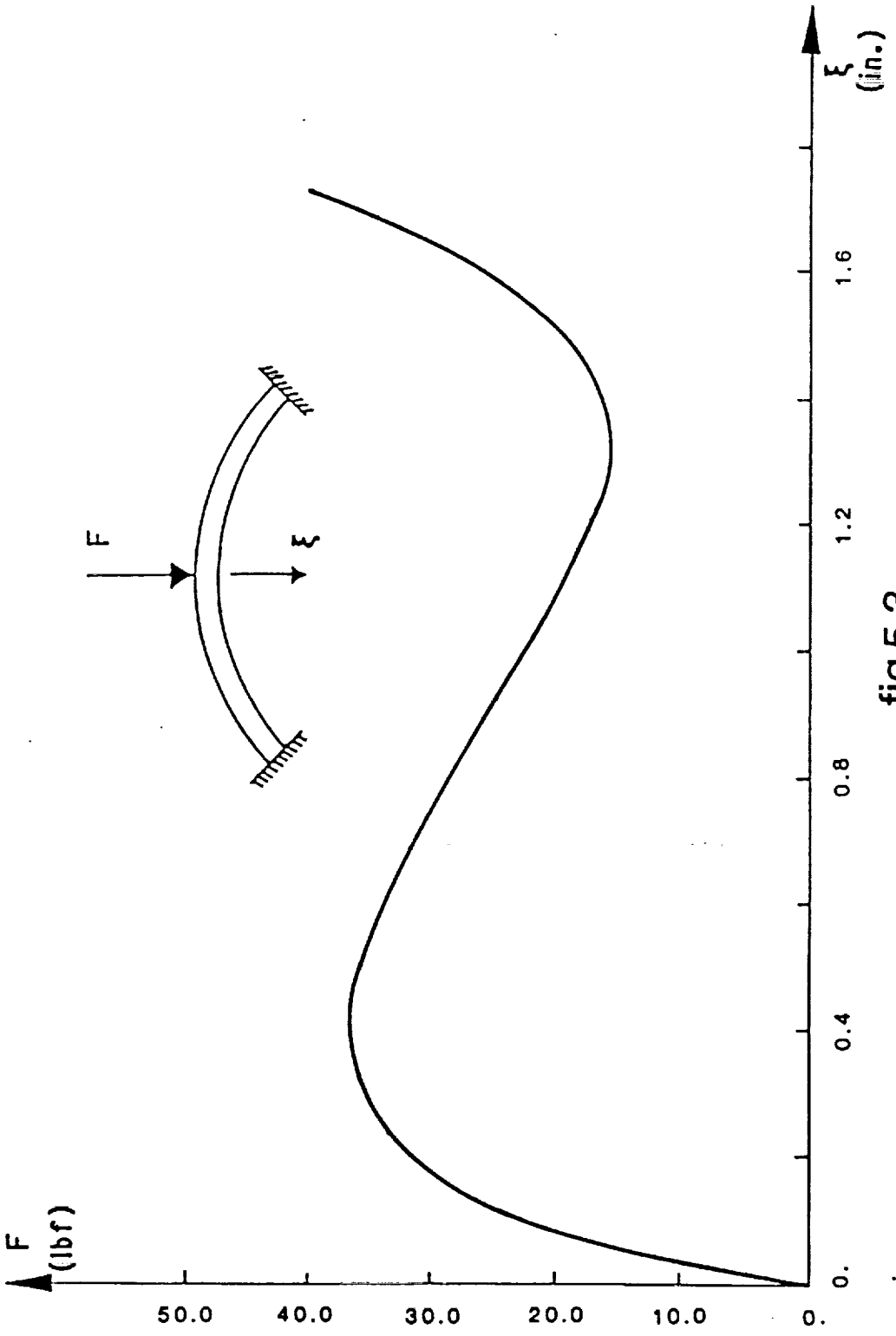

fig 5.3

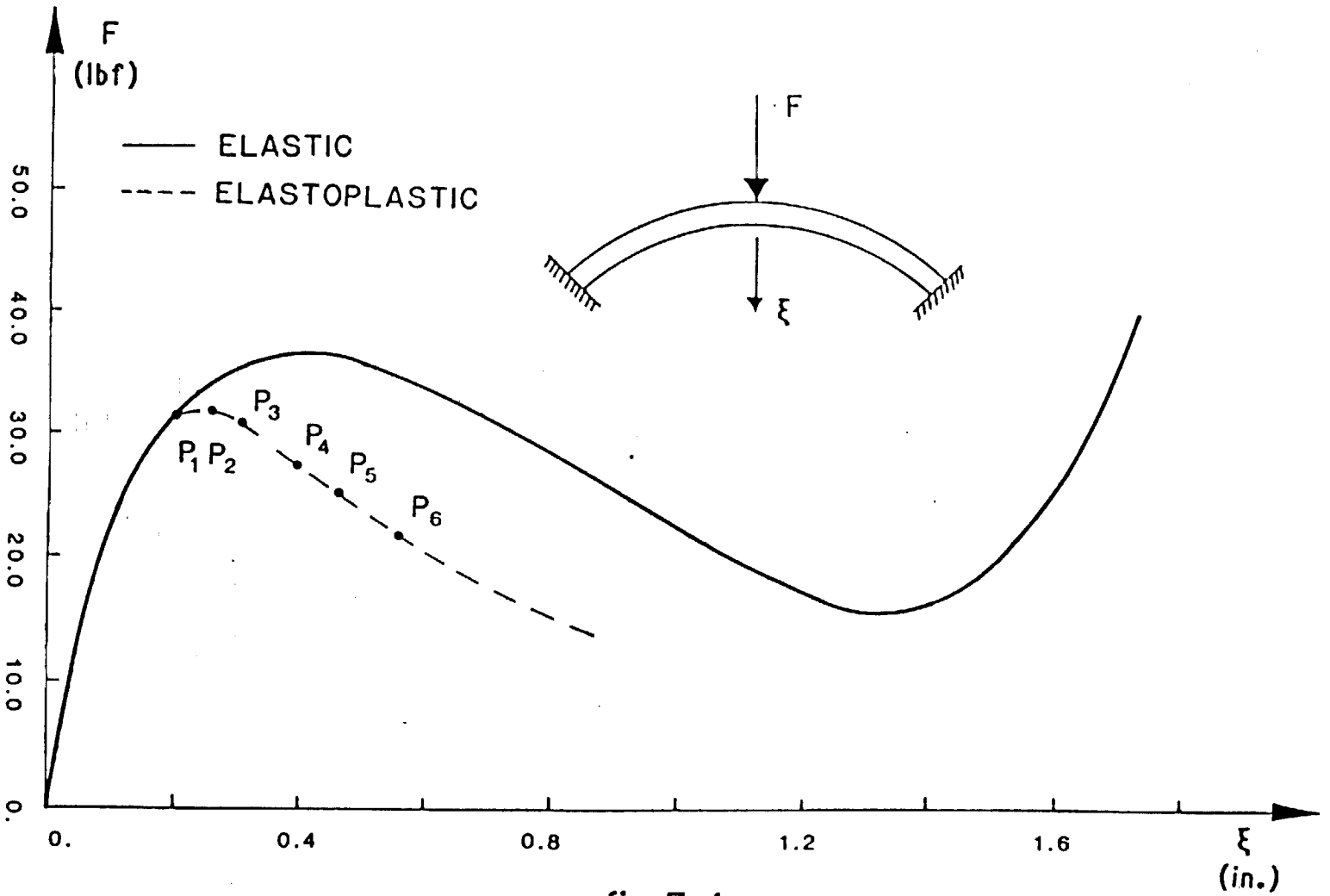
F
(lbf)
ELASTIC
ELASTOPLASTIC
50.0
40.0
30.0
20.0
10.0
0.
P1 P2
P3
P4
P5
P6
F
ξ
0.
0.4
0.8
1.2
1.6
ξ
(in.)

fig 5.4

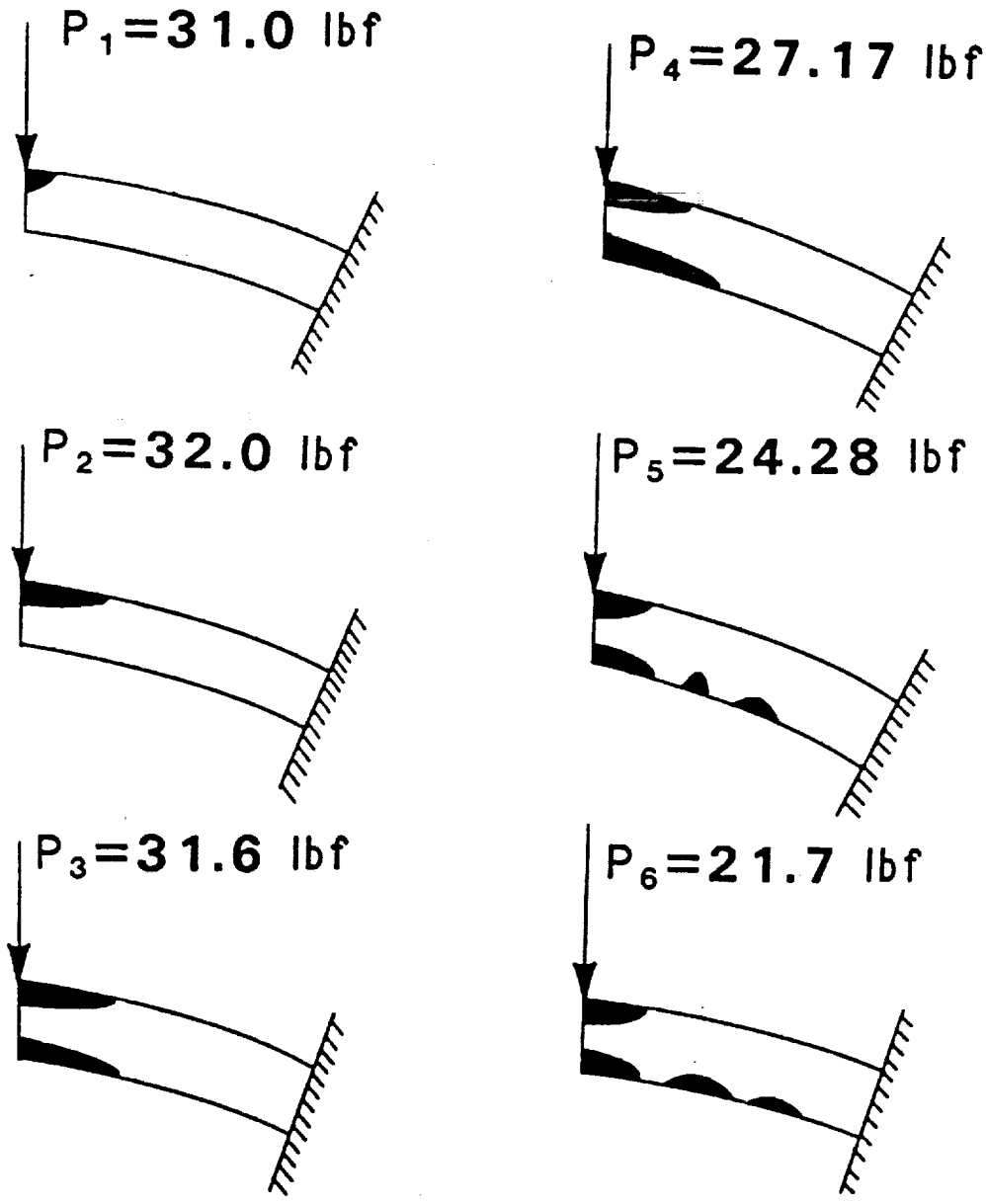
P1=31.0 lbf
P4=27.17 lbf
P2=32.0 lbf
P5=24.28 lbf
P3=31.6 lbf
P6=21.7 lbf

fig 5.5

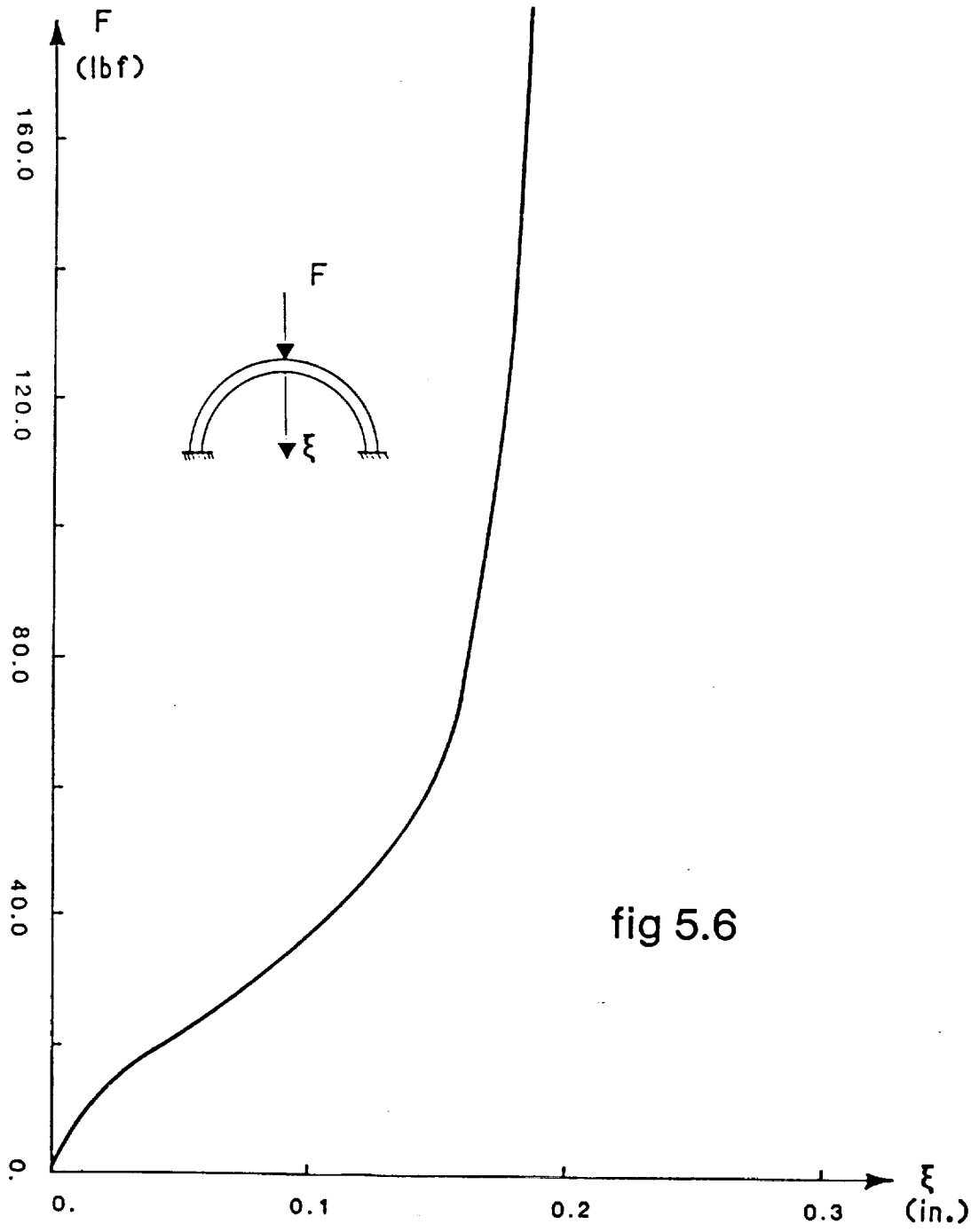

fig 5.6

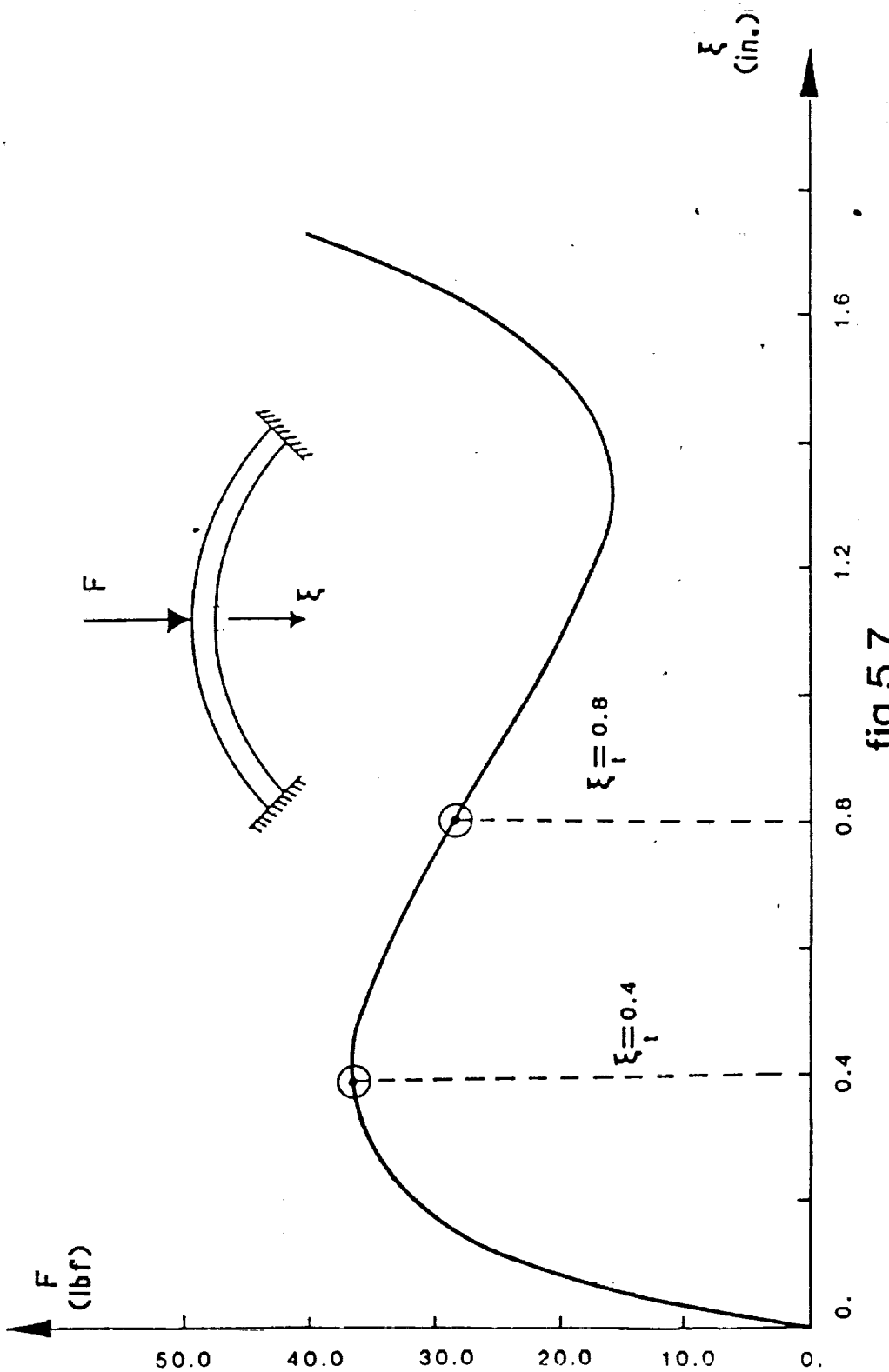

fig 5.7

LIST OF PAPERS PUBLISHED IN COURSE OF WORK

1. Padovan, J., Tovichakchaikul, S., "Self-Adaptive Predictor-Corrector Algorithms for Static Nonlinear Structural Analysis", Computer and Structures, Vol. 15, pp. 365, 1982.
2. Padovan, J. Tovichakchaikul, S., "On the Solution of Creep Induced Buckling in General Structure", Computers and Structures, Vol. 15, pp. 379, 1982.
3. Padovan, J., Arechaga, Tomas, "Formal Convergence Characteristics of Elliptically Constrained Incremental Newton Raphson Algorithm", International Journal of Engineering Science, Vol. 20, pp. 1077, 1982.
4. Padovan, J., Tovichakchaikul, S., "On the Solution of Elastic-Plastic Static and Dynamic Post-Buckling Collapse of General Structure", presented at Symposium on Advances and Trends in Structural and Solid Mechanics, Oct., 1982, Arlington, VA and Computers and Structures, Vol. 16, pp. 199, 1983.
5. Padovan, J., Archaga, T., "Formal Numerical Characteristics of Closed Constrained Incremental Successive Substitution Algorithms", Journal of the Franklin Institute, Vol. 314, pp. 143, 1982.
6. Padovan, J., Tovichakchaikul, S., "Self Adaptive Closed Constrained Solution Algorithms for Nonlinear Conduction", Numerical Heat Transfer, Vol. 5, pp. 253, 1982.
7. Tovichakchaikul, S., Padovan, J., "Pseudo-Updated Constrained Solution Algorithm for Nonlinear Heat Conduction", AIAA Journal, Vol. 21, 902-908, 1983.

8. Padovan, J., Tovichakchaikul, S., "Algorithms for Elasto-Plastic Creep Postbuckling", ASCE Structures Congress, Houston, Oct. 1983: also The Journal of Applied Mechanics, ASCE, Vol. 110, 911, 1984.

9. Padovan, J. and Pai, S.S., "Quasi Static Solution Algorithms for Kinematically/Materially Nonlinear Thermomechanical Problems", Journal of Thermal Stresses, Vol. 7, pp. 227-257, 1984.

10. Padovan, J. and Pai, S., "Extension of Constrained Incremental Newton Raphson Scheme to Generalized Loading Fields", Jr. of Franklin Institute, Vol. 318, No. 3, pp. 165-186, 1984.

11. Padovan, J. and Lackney, J., "On the Development of Hierarchical Solution Strategies for Nonlinear Finite Element Formulations", Computers and Structures, Vol. 19, pp. 535-544, 1984.

12. Padovan, J., Moscarello, R., Stafford, J. and Tabaddor, F., "Pantographing Self Adaptive Gap Elements", Computers and Structures, Vol. 20, pp. 745-758, 1985.

13. Padovan, J. and Lackney, J., "Hierarchical Implicit Dynamic Least Square Solution Algorithm", Jr. of Computers and Structures, Vol. 22, No. 3, pp. 479-489, 1986.

14. Padovan, J., Moscarello, R., "Locally Bound Constrained Newton Raphson Solution Algorithms, Computers and Structures, 23, 181-197, 1986.

15. Padovan, J., "Solving Postbuckling Collapse of Structures, Journal of Finite Elements in Analyses and Design, Vol. 1, 363-385, 1985.

16. Padovan, J. and Lackney, J., "Constrained Hierarchical Least Square Nonlinear Equation Solvers", Computers and Structures, Vol. 23, No. 2, pp. 251-263, 1986.

17. Padovan, J. and Krishna, L., "Multiply Scaled Constrained Nonlinear Equation Solvers", Numerical Heat Transfer, Vol. 10, pp. 463-482, 1986.

18. Padovan, J., "Steady and Transient Least Square Solvers for Thermal Problems", Numerical Heat Transfer, Vol. 12, pp. 263-284, 1987.

19. Padovan, J., "Multiply Constrained Partitioned Nonlinear Equation Solvers", Computational Mechanics, Vol. 3, pp. 255-273, 1988.

REPORT DOCUMENTATION PAGE

Form Approved
OMB No. 0704-0188

1. AGENCY USE ONLY (*Leave blank*)	2. REPORT DATE	3. REPORT TYPE AND DATES COVERED
	November 1991	Final Contractor Report

4. TITLE AND SUBTITLE

Self Adaptive Solution Strategies: Locally Bound Constrained Newton Raphson Solution Algorithms

5. FUNDING NUMBERS

WU-505-63-5B
G-NAG3-54

6. AUTHOR(S)

Joe Padovan

7. PERFORMING ORGANIZATION NAME(S) AND ADDRESS(ES)

University of Akron
Department of Mechanical Engineering
Akron, Ohio 44325-3903

8. PERFORMING ORGANIZATION REPORT NUMBER

None

9. SPONSORING/MONITORING AGENCY NAMES(S) AND ADDRESS(ES)

National Aeronautics and Space Administration
Lewis Research Center
Cleveland, Ohio 44135-3191

10. SPONSORING/MONITORING AGENCY REPORT NUMBER

NASA CR-189069

11. SUPPLEMENTARY NOTES

Project Manager, C.C. Chamis, Structures Division, NASA Lewis Research Center, (216) 433-3252.

12a. DISTRIBUTION/AVAILABILITY STATEMENT

Unclassified - Unlimited
Subject Category 39

12b. DISTRIBUTION CODE

13. ABSTRACT (*Maximum 200 words*)

This final report summarizes strategies developed during the course of work which enable the automatic adjustment of the constraint surfaces recently used to extend the range and numerical stability/efficiency of nonlinear finite element equation solvers. In addition to handling kinematic and material induced nonlinearity, both pre- and postbuckling behavior can be treated. The scheme developed employs localized bounds on various hierarchical partitions of the field variables. These are used to resize, shape, and orient the global constraint surface, thereby enabling essentially automatic load/deflection incrementation. Due to the generality of the approach taken, it can be implemented in conjunction with constraints of an arbitrary functional type. To benchmark the method, several numerical experiments are presented. These include problems involving kinematic and material nonlinearity, as well as pre- and postbuckling characteristics. Also included is a list of papers published in the course of the work. Overall a total of 19 papers were published in 9 different national and international journals.

14. SUBJECT TERMS

Finite element; Nonlinear analysis; Constraint surfaces; Postbuckling; Resize; Benchmark problems

15. NUMBER OF PAGES
76

16. PRICE CODE
A04

17. SECURITY CLASSIFICATION OF REPORT	18. SECURITY CLASSIFICATION OF THIS PAGE	19. SECURITY CLASSIFICATION OF ABSTRACT	20. LIMITATION OF ABSTRACT
Unclassified	Unclassified	Unclassified	

NSN 7540-01-280-5500

U.S. GOVERNMENT PRINTING OFFICE: 1992 - 648-034/40043

Standard Form 298 (Rev. 2-89)
Prescribed by ANSI Std. 739-18
298-102